Acknowledgments

The research was partially supported by a grant from the Ministry of Education, Science and Culture, Japan. A part of this work was undertaken at the Keio Integrated Medical Research Center.

Disclosure of Potential Conflicts of Interest

The authors indicate no potential conflicts of interest.

References

1 Boheler KR, Czyz J, Tweedie D et al. Differentiation of pluripotent embryonic stem cells into cardiomyocytes. Circ Res 2002;91:189–201.
2 Makino S, Fukuda K, Miyoshi S et al. Cardiomyocytes can be generated from marrow stromal cells in vitro. J Clin Invest 1999;103:697–705.
3 Orlic D, Kajstura J, Chimenti S et al. Bone marrow cells regenerate infarcted myocardium. Nature 2001;410:701–705.
4 Tomita S, Li RK, Weisel RD et al. Autologous transplantation of bone marrow cells improves damaged heart function. Circulation 1999;100:II247–II256.
5 Asahara T, Murohara T, Sullivan A et al. Isolation of putative progenitor endothelial cells for angiogenesis. Science 1997;275:964–967.
6 Tsuji H, Miyoshi S, Ikegami Y et al. Xenografted human amniotic membrane-derived mesenchymal stem cells are immunologically tolerated and transdifferentiated into cardiomyocytes. Circ Res 2010;106:1613–1623.
7 Terai M, Uyama T, Sugiki T et al. Immortalization of human fetal cells: The life span of umbilical cord blood-derived cells can be prolonged without manipulating p16INK4a/RB braking pathway. Mol Biol Cell 2005;16:1491–1499.
8 Takeda Y, Mori T, Imabayashi H et al. Can the life span of human marrow stromal cells be prolonged by bmi-1, E6, E7, and/or telomerase without affecting cardiomyogenic differentiation? J Gene Med 2004;6:833–845.
9 Hida N, Nishiyama N, Miyoshi S et al. Novel cardiac precursor-like cells from human menstrual blood-derived mesenchymal cells. Stem Cells 2008;26:1695–1704.
10 Nishiyama N, Miyoshi S, Hida N et al. The significant cardiomyogenic potential of human umbilical cord blood-derived mesenchymal stem cells in vitro. Stem Cells 2007;25:2017–2024.
11 Okamoto K, Miyoshi S, Toyoda M et al. 'Working' cardiomyocytes exhibiting plateau action potentials from human placenta-derived extraembryonic mesodermal cells. Exp Cell Res 2007;313:2550–2562.
12 Grauss RW, Winter EM, van Tuyn J et al. Mesenchymal stem cells from ischemic heart disease patients improve left ventricular function after acute myocardial infarction. Am J Physiol Heart Circ Physiol 2007;293:H2438–H2447.
13 Hou M, Yang KM, Zhang H et al. Transplantation of mesenchymal stem cells from human bone marrow improves damaged heart function in rats. Int J Cardiol 2007;115:220–228.
14 Chen SL, Fang WW, Ye F et al. Effect on left ventricular function of intracoronary transplantation of autologous bone marrow mesenchymal stem cell in patients with acute myocardial infarction. Am J Cardiol 2004;94:92–95.
15 Hare JM, Traverse JH, Henry TD et al. A randomized, double-blind, placebo-controlled, dose-escalation study of intravenous adult human mesenchymal stem cells (prochymal) after acute myocardial infarction. J Am Coll Cardiol 2009;54:2277–2286.
16 Matsushita K, Wu Y, Okamoto Y et al. Local renin angiotensin expression regulates human mesenchymal stem cell differentiation to adipocytes. Hypertension 2006;48:1095–1102.
17 Iwanami J, Mogi M, Li JM et al. Deletion of angiotensin II type 2 receptor attenuates protective effects of bone marrow stromal cell treatment on ischemia-reperfusion brain injury in mice. Stroke 2008; 39:2554–2559.
18 Ikegami Y, Miyoshi S, Nishiyama N et al. Serum-independent cardiomyogenic transdifferentiation in human endometrium-derived mesenchymal cells. Artif Organs 2010;34:280–288.
19 Shinmura D, Togashi I, Miyoshi S et al. Pretreatment of human mesenchymal stem cells with pioglitazone improved efficiency of cardiomyogenic transdifferentiation and improved cardiac function. Stem Cells 2010 (in press).
20 Kami D, Shiojima I, Makino H et al. Gremlin enhances the determined path to cardiomyogenesis. PLoS One 2008;3:e2407.
21 Gnecchi M, He H, Liang O et al. Paracrine action accounts for marked protection of ischemic heart by Akt-modified mesenchymal stem cells. Nat Med 2005;11:367–368.

See www.StemCells.com for supporting information available online.

CELLULAR REPROGRAMMING
Volume 13, Number 4, 2011

DOI: 10.1089/cell.2011.0004

Early Senescence Is Not an Inevitable Fate of Human-Induced Pluripotent Stem-Derived Cells

Maiko Gokoh,[1] Miwako Nishio,[1] Naoko Nakamura,[1] Satoko Matsuyama,[1] Masako Nakahara,[1] Shinnosuke Suzuki,[1] Masami Mitsumoto,[1] Hidenori Akutsu,[2] Akihiro Umezawa,[2] Kazuki Yasuda,[3] Akira Yuo,[1] and Kumiko Saeki[1]

Abstract

Human-induced pluripotent stem cells (hiPSCs) are expected to become a powerful tool for regenerative medicine. Their efficacy in the use of clinical purposes is currently under intensive verification. It was reported that hiPSC-derived hemangioblasts had severely limited expansion capability due to an induction of early senescence: hiPSC-derived vascular endothelial cells (VECs) senesced after one passage and hiPSC-derived hematopoietic progenitor cells (HPCs) showed substantially decreased colony-forming activities. Here we show that early senescence is not an inevitable fate of hiPSC-derived cells. Applying our unique feeder-free culture methods for the differentiations of human embryonic stem cells (hESCs), we successfully generated VECs and HPCs from three lines of hiPSCs that were established by using a retrovirus vector system. All hiPS-derived VECs could be subcultured by 2:1 ~ 3:1 dilutions up to 10 ~ 20 passages, after which the cells underwent senescence. Among the three lines of hiPSCs, two lines generated HPCs that bore comparable granulocyte colony-forming units to those of hESCs. Moreover, one line effectively reproduced HPCs within the sac-like structures, the fields of *in vitro* hematopoiesis, as in the case of hESCs. Surprisingly, release of neutrophils into culture supernatant persisted even longer (~60 days) than the case of hESCs (~40 days). Thus, the problem of early senescence can be overcome by selecting appropriate lines of hiPSCs and applying proper differentiation methods to them.

Introduction

HUMAN INDUCED PLURIPOTENT STEM CELLS (hiPSCs) hold great promise for the development of regenerative medicine with their unlimited expansion capacities and pluripotency that were equivalent to human embryonic stem cells (hESCs). Before translating the achievements of basic researches to medical purposes, however, the efficacy and safety of hiPSCs must be carefully scrutinized from various points of view. Large quantities of useful findings have been accumulating in the case of murine iPSCs (miPSCs); however, performing the studies on hiPSCs is particularly important because hiPSCs may not be the real equivalent of miPSCs as the hESCs may not be the genuine counterpart of murine ESCs (mESCs) (Tesar et al., 2007; Vallier et al., 2009).

So far, two major issues have been raised concerning the disadvantageous outcomes of iPSCs after differentiation. One is a widely recognized matter of tumorigeneity, which was reported in the cases of miPSC chimeric mice (Okita et al., 2007) and the mice transplanted with miPSC-derived differentiated cells (Nelson et al., 2009). Already, several measures have been proposed to overcome this problem: an application of nonviral vectors (Okita et al., 2008; Yu et al., 2009), excisions of integrated transgenes (Kaji et al., 2009; Woltjen et al., 2009), a usage of L-myc instead of c-myc transgene (Nakagawa et al., 2008, 2010), and a selection of iPSC lines with least tumorigeneity after differentiation (Miura et al., 2009). Those strategies, along with the recent technological innovations to introduce the reprogramming factors via RNA-based (Fusaki et al., 2009; Seki et al., 2010; Warren et al., 2010) or protein-based systems (Kim et al., 2009; Zhou et al., 2009), are expected to make a great contribution toward the complete resolution of the problem.

[1]Department of Disease Control, National Center for Global Health and Medicine, Tokyo, Japan.
[2]Department of Reproductive Biology, National Research Institute for Child Health and Development, Tokyo, Japan.
[3]Department of Metabolic Disorder, National Center for Global Health and Medicine, Tokyo, Japan.

The second issue is rather a newly proposed one: an induction of early senescence in hiPSC-derived differentiated cells (Feng et al., 2010). It was reported that every hiPSC established by using a retrovirus vector system suffered from expansion deficiency after differentiation into vascular endothelial cells (VECs), hematopoietic progenitor cells (HPCs), and retinal pigmented epithelium cells (Feng et al., 2010). Although the molecular mechanism of early senescence remains elusive, the effects of p53 inactivation, LIN28 activation and insertion of proviral transgenes into chromosomes were discussed (Feng et al., 2010). The finding of early senescence is worth reporting in that it has provoked a caution that we should o use during our researches on hiPSCs. Nevertheless, we thought that their conclusion must be further validated in other situations, where differentiation processes are performed by distinct methods, because early senescence is often caused by cellular stresses and the degrees of stresses substantially vary depending on culture conditions.

We previously established feeder-free methods for neutrophilic (Saeki et al., 2009) and vascular endothelial (Nakahara et al., 2009) differentiations of hESCs. By applying those methods to hiPSCs, we studied the incidence of early senescence during the differentiation of hiPSCs that were established by using a retroviral vector system. Our data indicate that early senescence is not an inevitable fate of the hiPSC-derived differentiated cells even in the presence of retroviral insertions of the reprogramming transgenes. We also show that hiPSC-derived VECs undergo senescence after 10~20 passages, as in the cases of primary human VECs, without entering crisis. Our results clearly show that the problem of early cellular senescence can be overcome by selecting appropriate lines of hiPSCs and applying proper differentiation methods to them.

Materials and Methods

Cell culture

The use of hESCs was performed in accordance with the Guidelines for Derivation and Utilization of Human Embryonic Stem Cells of the Ministry of Education, Culture, Sports, Science, and Technology (MEXT) of Japan, after approval by the institutional review board of International Medical Center of Japan (IMCJ). The hESCs (KhES-1, KhES-3) (Suemori et al., 2006) were provided by Kyoto University (Kyoto, Japan). The hiPSC were provided by either CiRA at Kyoto University (253G1 and 253 G4 (Nakagawa et al., 2008), 201B7 and 201B2 (Takahashi et al., 2007) or by National Research Institute for Child Health and Development (#25). The cells were maintained on dishes coated with γ-irradiated murine embryonic fibroblasts (MEFs) in DMEM/F12 (Invitrogen Corp., Carlsbad, CA) supplemented with 20% Knockout™ Serum Replacement (KSR) (Invitrogen Corp.), 5 ng/mL fibroblast growth factor 2 (FGF-2; Pepro Tech Inc., Rocky Hill, NJ), 1% nonessential amino acids solution (Invitrogen Corp.), 1 mM sodium pyruvate solution (Invitrogen Corp.), 100 μM 2-mercaptethanol (Sigma Chemical Co., St. Louis, MO), 2 mM L-glutamine (Invitrogen Corp.), 20 U/mL penicillin (Invitrogen Corp.) and 20 μg/mL streptomycin (Invitrogen Corp.). The cells were passed twice a week (e.g., on Tuesday mornings and Friday evenings) by a treatment with dissociation liquid, which contains 0.25% trypsin (Invitrogen Corp.), 1 mg/mL collagenase IV (WAKO Pure Chemical Industries, Osaka, Japan), 20% KSR, 1 mM $CaCl_2$, at 37°C for 5 to 15 min and seeded at split ratios of 1:2 to 1:4 into new MEF-coated dishes. During the course of experiments, cells showed normal karyotypes.

Vascular endothelial differentiation of hESCs/hiPSCs

Differentiation was performed as previously described (Nakahara et al., 2009) with a slight modification. The hESCs/hiPSCs were detached from culture plates by using the dissociation liquid for 15 min at 37°C. The mildly dissociated hESC/iPSC clumps were cultured in a 6-cm diameter low-attachment dish (Nalge Nunc International K.K., Tokyo, Japan) to form spheres using the differentiation medium consisting Iscove's modified Dulbecco's medium (IMDM) (Sigma Chemical Co.) supplemented with 15% heat-inactivated fetal bovine serum (FBS) (PAA Laboratories GmbH, Linz, Austria), 0.1 mM 2-mercaptoethanol, 3 mM L-glutamine, 10 U/mL penicillin, 20 ng/mL vascular endothelial growth factor (VEGFA), 20 ng/mL bone morphogenetic protein 4 (BMP4), 20 ng/mL stem cell factor (SCF), 10 ng/mL FMS-related tyrosine kinase-3 ligand (Flt3-L), 20 ng/mL Interleukin 3 (IL3), and 10 ng/mL IL6. After incubation for 3 days at 37°C under a 100% humidified condition in a 5% CO_2 gas incubator, spheres were subjected to adherent culture using 100 mm×20 mm 0.1% porcine type A gelatin (Sigma Chemical Co.)-coated dishes in the differentiation medium described above. Media were changed twice a week. For passage, cells were harvested by treatment with 0.25% trypsin and 1 mM EDTA and replated at split ratios of 1:2 on new gelatin-coated dishes.

Senescence-associated (SA)-β-galactosidase assays

The 1×10^5 VECs were cultured in 6-cm culture plates. After an incubation at 37°C in 5% CO_2 incubator for 4~5 days, cells were subjected to SA-β-galactosidase assays by using Senescence Detection Kit (BioVision Research Products Inc., Mountain View, CA) according to a manufacture's guidance.

Cord formation assays

Matrigel™ Basement Membrane Matrix, phenol-Red free (Cat 356237, BD Biosciences, San Jose, CA) was loaded into the 24 multiwell dishes (95 μL/well). After the dishes were incubated for 30 min at 37°C, 1×10^4 cells per well were seeded in differentiation medium described above. Cell morphologies were observed after overnight culture under an inverted light microscope (Olympus Optical Co. Ltd, Japan).

Uptake of acetylated low-density lipoprotein (Ac-LDL)

Cells were transferred in four-well chamber slide system (Nalge Nunc International Corp., Naperville, IL). After overnight culture, cells were washed by Hank's balanced salt solution (HBSS) twice and incubated in serum-free medium containing 10 μg/mL of low-density lipoprotein from human plasma, acetylated, DiI complex (DiI Ac-LDL) (Invitrogen Corp.) for 4 h. After washing the cells by HBSS for three times, nuclei were counterstained using 10 nM of Hoechst 33342 (Sigma Chemical

Co.). After washing the cells, samples were observed under the fluorescence microscope (Olympus Optical Co. Ltd).

Flow cytometry

Cells were collected by a treatment with 0.2% EDTA or Dispase (BD Biosciences). After a wash in phosphate-buffered saline (PBS), 1×10^6 cells were reacted with first antibodies on ice for 30 min. The expression level of each protein was analyzed using a FACSCalibur™ (BD Biosciences). The antibodies used were a mouse monoclonal antihuman Tie-2- allophycocyanin (APC) antibody (R&D Systems Inc., Minneapolis, MN), antihuman VEGF receptor 1 (VEGF R1)-PE antibody (R&D Systems Inc.), mouse antihuman CD45-PE (BD Biosciences), and mouse antihuman CD11b-PE (BD Biosciences). After antibody-staining procedures, cells were stained with propidium iodide (PI) (Sigma Chemical Co.), in the case of Tie-2 staining, or TO-PRO3 fluorescent dye (Invitrogen Corp.), in the cases of VEGF1, CD45, and CD11b staining, for 10 min. During analysis, dead cells were gated out as FL-2 higher fractions, in the case of PI staining, or FL4-higher fractions in the case of TO-PRO3 staining.

Immunostaining

The cells were fixed on slide glasses by using a cytospin apparatus (Cytospin 2) along with further fixation with acetone/methanol solution (1:3). The immunostaining procedure was performed as described elsewhere (Nakahara et al., 2009) with first antibody reactions using a rabbit polyclonal antihuman $p16^{INK4A}$ antibody (SC-20) (Santa Cruz Biotechnology Inc., Santa Cruz, CA), a mouse monoclonal antihuman $p21^{CIP1}$ antibody (Santa Cruz Biotechnology Inc.), a rabbit polyclonal antihuman endothelial nitric oxide synthase (eNOS) antibody (H-159) (Santa Cruz Biotechnology Inc.), or a rabbit polyclonal antihuman von Willebrand factor (vWF) antibody (Sigma Chemical Co.), followed by second antibody reactions using Alexa Fluor® 488 chicken antimouse IgG (H+L), Alexa Fluor® 568 goat antirabbit IgG (H+L), or Alexa Fluor® 594 chicken antigoat IgG (H+L) (Invitrogen Corp.). Nuclear counterstaining was performed using 300 nM of 4′,6-diamino-2-phenylindole (DAPI).

Hematopoietic differentiation of hESCs/hiPSCs

Differentiation was performed as previously described (Saeki et al., 2009). In brief, hESCs/hiPSCs were detached with 1 mg/mL collagenase IV (Invitrogen Corp.) and transferred to a 6 cm diameter low-attachment dish (Nalge Nunc International K.K.) coated with 2-methacryloyloxyethyl phosphorylcholine in 5 mL IMDM (Sigma Chemical Co.) supplemented with 15% FBS (PAA Laboratories GmbH), 2 mM L-glutamine, 100 μM 2-mercaptethanol, 20 U/mL penicillin, and 20 μg/mL streptomycin in the presence of 20 ng/mL insulin-like growth factor II (IGF-II; Pepro Tech Inc.), 20 ng/mL VEGFA (Pepro Tech Inc.), 100 ng/mL SCF (Pepro Tech Inc.), 100 ng/mL Flt3-L (Pepro Tech Inc.), 50 ng/mL thrombopoietin (TPO; Kirin Brewery Company, Ltd., Tokyo, Japan), and 100 ng/mL G-CSF (Kirin Brewery Company, Ltd.) (Differentiation medium) at a density of 4×10^5 cells/mL. After primary differentiation for 3 days, the spheres were transferred to 10-cm diameter dish coated with 0.1% gelatin. Spheroid cells floating in the culture supernatant were collected over time and analyzed.

Colony assays

Colony assays were performed using Methocult TM GF^+H4535 (Stemcell Technologies Inc., Vancouver, Canada) in accordance with the manufacturer's recommendations. In brief, 0.3 mL of cell suspension, which contained 10 cells, was mixed in 3 mL of methylcellulose solution consisting of 1% methylcellulose, 30% FBS, 1% bovine serum albumin, 100 μM 2-mercaptoethanol, 2 mM L-glutamine, 50 ng/mL SCF (Pepro Tech Inc.), 20 ng/mL interleukin 3 (IL-3; Pepro Tech Inc.), 20 ng/mL interleukin 6 (IL-6; Pepro Tech Inc.), 20 ng/mL granulocyte-macrophage colony-stimulating factor (GM-CSF; Pepro Tech Inc.), 20 ng/mL G-CSF and 3 U/mL erythropoietin (Kirin Brewery Company, Ltd.) in 3.5-cm culture dishes. After 2 weeks, the number of colonies was counted. The morphology of the colonies was observed using an inverted light microscope (Olympus Optical Co. Ltd).

Reverse transcription-polymerase chain reaction (RT-PCR)

RNA was extracted from 5×10^6 cells using an RNeasy Mini Kit (Qiagen Inc., Valencia, CA) and cDNA was synthesized using a Superscript II Kit (Invitrogen Corp.) in accordance with the manufacture's protocol. The sequence of the primers used are as follows: vascular endothelial (VE)-cadherin; a forward primer 5′-TGGGCTCAGACATC CACATA-3′ and a reverse primer 5′-TCACAGTCTCCCA TTGGGAAT-3′, platelet endothelial cell adhesion molecule-1 (PECAM1); a forward primer 5′-GCAAAATGGGAAGA ACCTGA-3′ and a reverse primer 5′-CACTCCTTCCAC CAACACCT-3′, interferon α1 (IFNA1); a forward primer 5′-GGAGTTTGATGGCAACCAGT-3′ and a revsese primer 5′-CTCTCCTCCTGCATCACACA-3′, interferon α2 (IFNA2); a forward primer 5′-GCAAGTCAAGCTGCTCTGTG-3′ and a reverse primer 5′-GATGGTTTCAGCCTTTTGGA-3′, interferon β1(IFNB1); a forward primer 5′-ATTGCCTCAAG GACAGGATG-3′ and a reverse primer 5′-AGCCAGGAGG TTCTCAACAA-3′. As a molecular maker, DNA MW Standard Marker 100 bp DNA Ladder (Takara Shuzo Co. Ltd., Shiga, Japan) was used.

Wright-Giemsa (WG) staining and special staining procedures

Viable cells in the dishes were observed directly using an inverted phase contrast light microscope (Olympus Optical Co. Ltd., Tokyo, Japan). Alternatively, the cells were fixed on glass slides using a cytospin centrifuge (Cytospin 2, SHANDON, Pittsburgh, PA), stained with WG solution (Muto Pure Chemical Co., Tokyo, Japan), and then observed using a light microscope (Olympus Optical Co. Ltd.). Double esterase staining was performed using the staining kit (Muto Pure Chemical Co.) according to the manufacturer's protocols.

Phagocytosis

hESC-derived neutrophils attracted to the lower chamber of Chemotaxel were suspended in HBSS containing 2.5% FBS

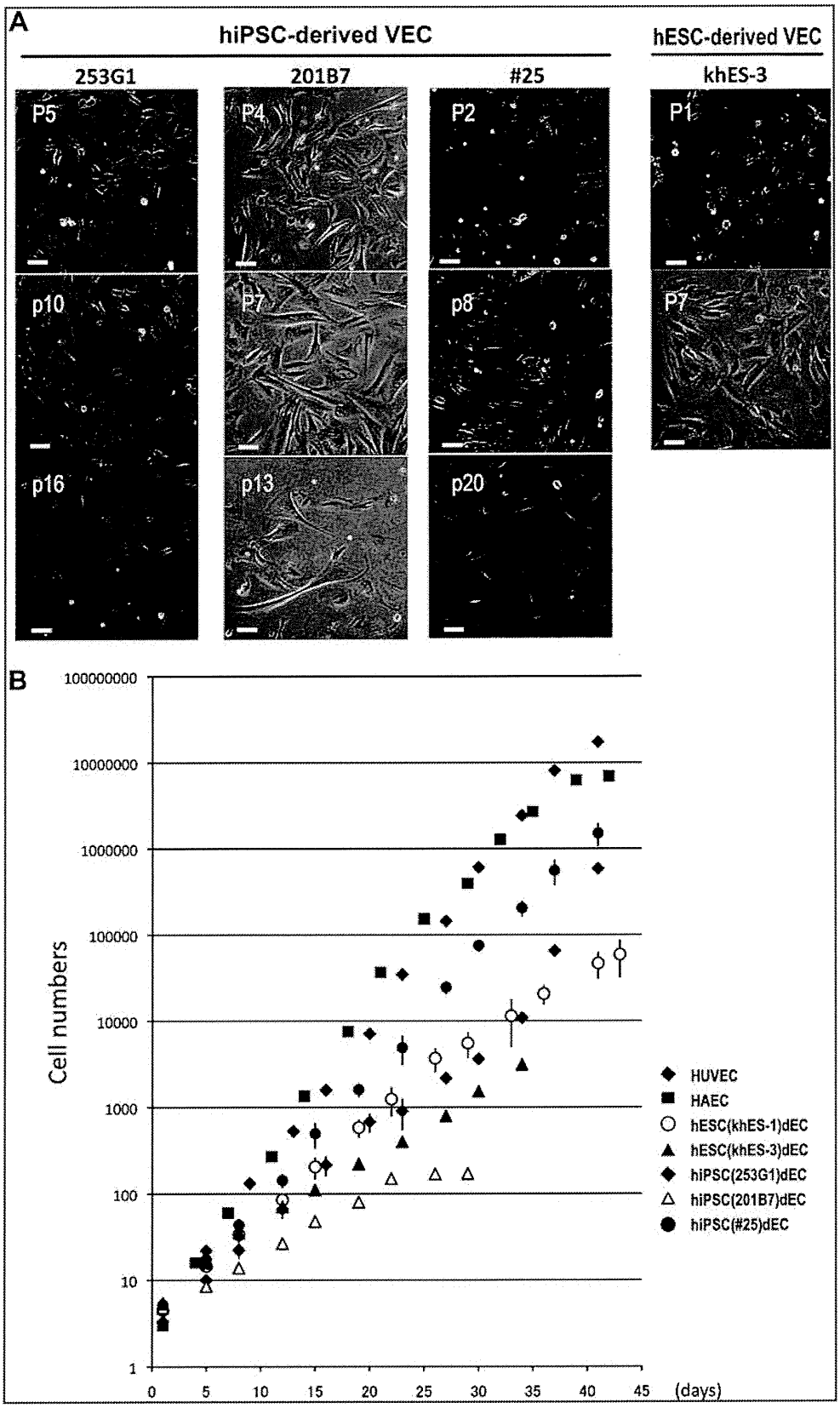
A
hiPSC-derived VEC
hESC-derived VEC
253G1
201B7
#25
khES-3
P5
P4
P2
P1
p10
P7
p8
P7
p16
p13
p20
B
Cell numbers
100000000
10000000
1000000
100000
10000
1000
100
10
1
0
5
10
15
20
25
30
35
40
45
(days)
HUVEC
HAEC
hESC(khES-1)dEC
hESC(khES-3)dEC
hiPSC(253G1)dEC
hiPSC(201B7)dEC
hiPSC(#25)dEC

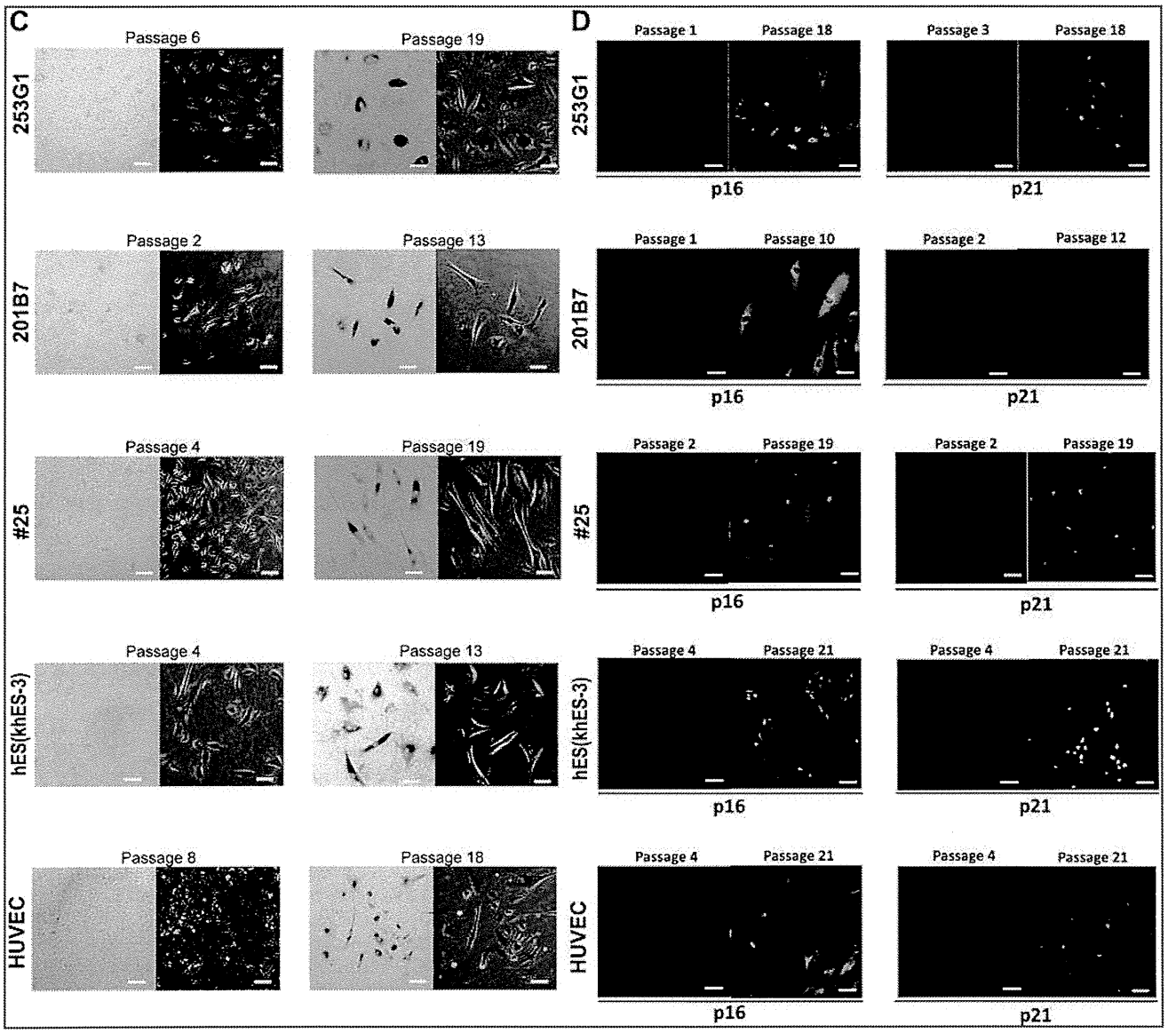

FIG. 1. (Continued).

and incubated at 37°C for 1 h with 5 μL zymosan (1 mg/mL) in the presence of 100 nM fMLP. Subsequently, the cells were collected using a cytospin apparatus and stained with WG solution. Phagocytosis was determined by a microscope observation.

Nitroblue tetrazolium reduction assay for respiratory burst activity

The floating cells were collected by mild centrifugation of the culture supernatant. After washing with PBS, the cells

FIG. 1. The VEC differentiation of hiPSCs. (**A**) Phase contrast micrographs. Morphologies of hiPSC-derived and hESC-derived VECs were shown as indicated. Numbers on the photographs in white letters indicates the passage number of each VEC. Scale bars indicate 100 μm. (**B**) Growth curves of various VECs. Average data with standard deviations from three independent experiments are shown in the cases of hiPSC(253G1)-derived VECs (closed triangles), hiPSC(201B7)-derived VECs (open triangles), hiPSC (#25)-derived VECs (gray circles), and hESC(khES-1)-derived VECs (open circles), whereas typical results from one or two experiments were shown in the cases of HUVEC (gray diamonds), HAEC (closed squares), and hESC(khES-3)-derived VECs (gray triangles). (**C**) SA-β-galactosidase assays. The hiPSC (253G1, 201B7, and #25)-derived VECs, hESC (khES-3)-derived VECs, and HUEVC at indicated passage numbers were subjected to SA-β-galactosidase assays. Scale bars indicate 100 μm. (**D**) Expressions of senescence-associated genes. The hiPSC (253G1, 201B7, and #25)-derived VECs, hESC (khES-3)-derived VECs, and HUEVC at indicated passage numbers were subjected to immunostaining studies using an anti-p16 or anti-p21 antibody as indicated. Scale bars indicate 100 μm.

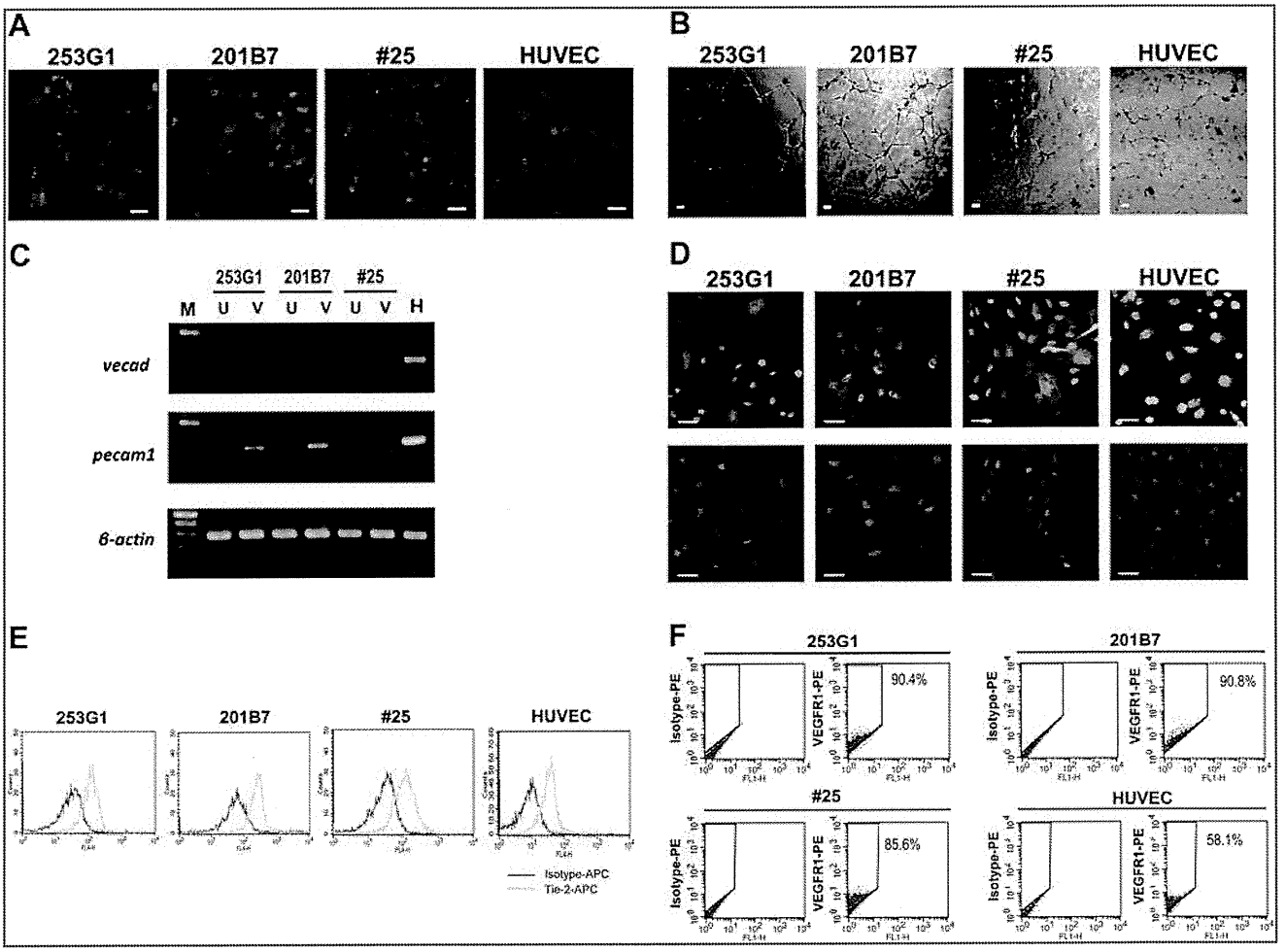

FIG. 2. Evaluation of hiPSC-derived VECs. (**A**) Ac-LDL-uptaking assays. VECs derived from each hiPSC line (253G1, 201B7, and #25) and HUEVC were subjected to Ac-LDL-uptaking assays (red; dil-Ac-LDL, blue; nuclear staining by Hoechst dye). Scale bars indicate 100 μm. (**B**) Cord formation assays. VECs derived from each hiPSC line (253G1, 201B7, and #25) and HUEVC were subjected to cord formation assays. Scale bars indicate 20 μm. (**C**) RT-PCR analyses. The message expressions of VE-cadherin (vecad), PECAM1 (pecam1), and β-actin were determined by RT-PCR in undifferentiated hiPSCs (253G1, 201B7, and #25), as indicated "U," or VEC-differentiated hiPSCs, as indicated "V." As positive control, cDNA of HUVEC was used as indicated "H." "M" indicates the molecular marker. (**D**) The expressions of the eNOS protein. The hiPSCs (253G1, 201B7, and #25 as indicated)-derived VECs and HUVEC were subjected to immunostaining studies using an antihuman eNOS antibody with nuclear counterstaining by DAPI. Scale bars indicate 50 μm. (**E, F**) The expressions of Tie-2 and VEGFR1 proteins. The VECs generated from hiPSCs (253G1, 201B7, and #25 as indicated) an HUVEC were subjected to flow cytometric analyses using an antihuman Tie-2 antibody (**E**) or an antihuman VEGFR1 antibody (**F**). A typical result from two to five experiments are shown.

were resuspended in 1 mL RPMI 1640 (Sigma Chemical Co.) supplemented with 10% FBS containing 1 mg/mL nitroblue tetrazolium (NBT) (Nacalai Tesque Inc., Kyoto, Japan) and 100 nM fMLP for 30 min at 37°C. After washing with PBS, the cells were resuspended in 10 μL PBS and dropped onto Matsunami Adhesive Silane (MAS)-coated glass slides (Matsunami Glass Ind., Ltd. Osaka, Japan) and the formazan blue-black deposit-containing cells were observed using a light microscope (Olympus Optical Co. Ltd.).

Results

hiPSC can generate subculturable VECs

We previously established a feeder-free method for the vascular endothelial differentiation of hESCs (Nakahara et al., 2009). The unique points of our method are (1) it is a two-tired differentiation system with a sphere-forming floating culture and a subsequent attachment culture, (2) it uses multiple hematopoietic cytokines in addition to a conventionally used cytokine of VEGF, (3) it enables high-purity production of VECs without contamination by growth-competing pericytes, (4) it enables the production of VECs that can be subcultured up to 10~20 passages (Nakahara et al., 2009). Applying this method, we performed VEC differentiation of the following lines of hiPSCs: 253G1 and 253G4, which were established from adult human dermal fibroblasts by introducing three retroviral transgenes of oct4, sox2, and klf-4 (OSK) (Nakagawa et al., 2008), 201B7 and 201B2, which were established from adult human dermal fibroblasts by introducing four retroviral transgenes of oct4,

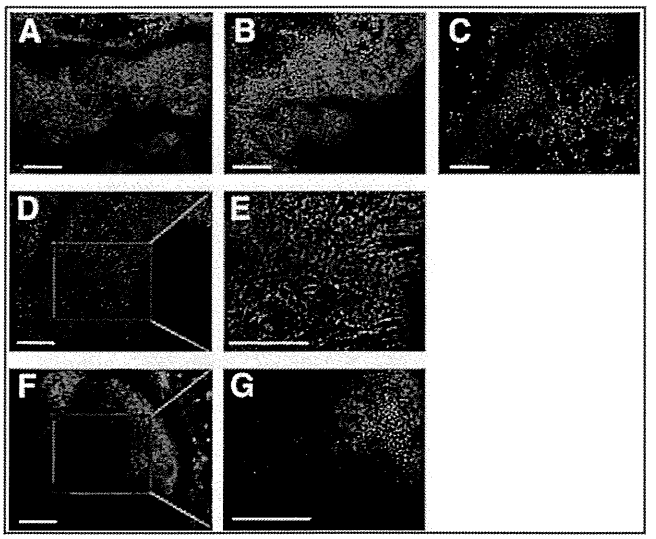

FIG. 3. Phase contrast microscopic observation during hematopoietic differentiation of hiPSCs. (**A–C**) Micrographs of the sac-like structures generated from 253G1 (**A**), 201B7 (**B**), and #25 (**C**). (**D**, **E**) Micrographs of the sac-like structures of 253G1 several days after manually puncturing the sac walls and releasing the inner hematopoietic cells. Note that the sac remained empty (**E**). (**F**, **G**) Micrographs of the sac-like structures of #25 several days after manually puncturing the sac walls and releasing the inner hematopoietic cells. Note that the sacs were refilled with hematopoietic cells (**G**). Scale bars indicate 200 μm.

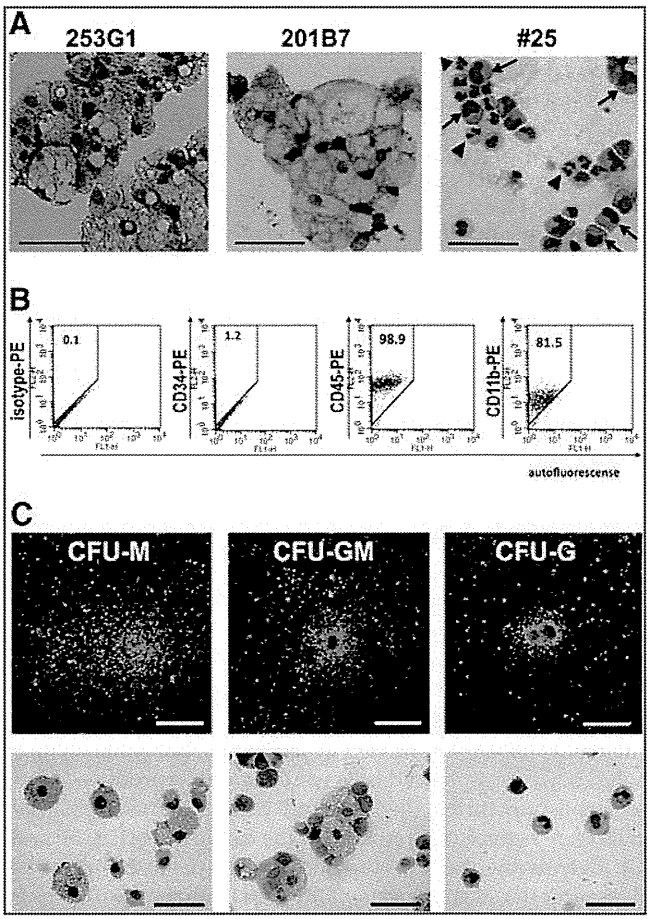

FIG. 4. Evaluation of hematopoietic potentials of hiPSC-derived cells (**A**) Cytological observation. Hematopoietic cells generated from hiPSCc (253G1, 201B7, and #25 as indicated) were stained by Wright-Giemsa solution. In #25-derived cells (right), azure granule-positive myeloid precursor cells (arrows) and segmented neutrocytes (arrow heads) were observed, whereas only macrophages were detected in 253G1-derived (left) and 201B7-derived (middle) cells. Scale bars indicate 50 μm. (**B**) Flow cytometry. The #25-derived hematopoietic cells were subjected to flow cytometric analyses using antihuman CD34, CD45, and CD11b antibodies as indicated. Number on each figure indicates the percentage of the corresponding marker-positive cells. (**C**) Colony assays. The #25-derived hematopoietic cells were subjected to colony assays. CFU-M, CFU-GM, and CFU-G were determined by phase contrast microscopic observation (upper panels; scale bars indicate 500 μm), which were further confirmed by Wright-Giemsa staining studies (lower panels; scale bars indicate 50 μm).

sox2, klf-4, and c-my (OSKM) (Takahashi et al., 2007) and #25, which were established from human embryonic lung fibroblasts of MRC-5 by introducing retroviral transgenes of OSKM.

Among the five lines, 253G1, 201B7, and #25 successfully generated VECs. Although cell morphologies slightly differed from one another (Fig. 1A), we could effectively expand the VECs generated from all the three lines: the hiPSC-derived VECs were subcultured by 2:1 ~ 3:1 dilutions up to 10 passages, in the case of 201B7, or even higher, in the cases of 253G1 and #25 (Fig. 1B). Both 253G1-derived and #25-derived VECs expanded with comparable growth rates to hESCs-derived VECs, whereas the growth speed of 201B7-derived VECs was slightly lower. After 10 ~ 20 passages, the hiPSC-derived VECs underwent senescence as demonstrated by SA-β-galactosidase assays as in the cases of hESC-derived VECs and HUVEC (Fig. 1C). In agreement with this, the expressions of senescence-associated gene products of $p16^{INK4A}$ and/or $p21^{CIP1}$ were induced in the senesced cells (Fig. 1D). Using the cells at exponentially growing phases, we evaluated the functions and maker expressions. All the hiPSC-derived VECs showed high Ac-LDL-uptaking capacities (Fig. 2A) and cord-forming activities (Fig. 2B). Although the expressions of VE-cadherin and PECAM1 messages were hardly detectable in #25-derived VECs (Fig. 2C), these cells showed comparable protein expressions of eNOS (Fig. 2D), Tie-2 (Fig. 2E), and VEGFR1 (Fig. 2F) to the other hiPSCs-derived VECs and HUVEC.

Thus, hiPSCs can generate VECs with equivalent expansion potentials to hESCs, although maturation levels of hiPSCs-derived VECs vary depending on the lines of hiPSCs.

hiPSCs can generate reproducible HPCs with comparable colony-forming activities to hESCs

We previously established a feeder-free method for the neutrophil differentiation of hESCs (Saeki et al., 2009). By our system, HPCs are generated within a unique construction named the "sac-like structure." Within this structure, HPCs are repeatedly generated: they are reproduced within a few days after manually puncturing the sac walls and releasing the inner HPCs into the culture supernatant (Saeki et al., 2009). The reproduction process can be repeated three or four times (Saeki et al., 2009).

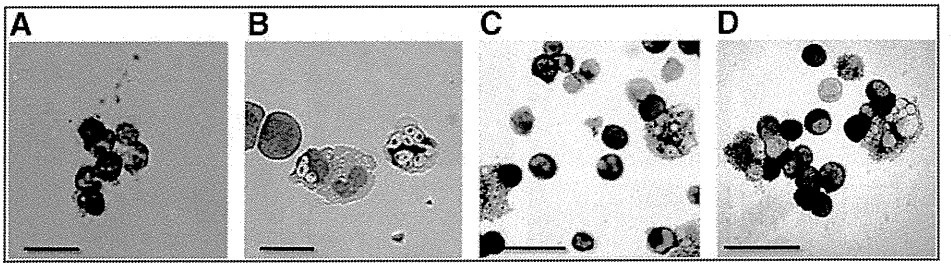

FIG. 5. Functional assessments and special staining. (**A, B**) The #25-derived hematopoietic cells were subjected to an NBT-reducing assay (**A**) or phagocytosis assay (**B**). Almost all the cells showed NBT-reducing activities (**A**) and zymosan-phagocytizing myeloid cells were often observed (**B**). Scale bars indicate 20 μm. (**C, D**) The #25-derived hematopoietic cells (**C**) or hESC (khES-3)-derived hematopoietic cells (**D**) were subjected to double esterase staining assay. Note that typical neutrophil-specific dark blue staining patterns were clearly observed in #25-derived cells, whereas hESC-derived hematopoietic cells showed rather mixed (brownish blue) staining patterns. Scale bars indicate 50 μm.

By applying this method, we performed neutrophil differentiation of 251G3, 201B7, and #25. All three lines successfully generated sac-like structures that were filled with abundant spheroid cells (Fig. 3A–C). However, the walls of 201B7-derived sacs seemed rather fragile because the inner spheroid cells spontaneously permeated the sac-like structures (Fig. 3B). Furthermore, we failed in reproducing spheroid cells after manually puncturing the sac walls and releasing inner spheroid cells into the culture supernatant (data not shown). In the case of 253G1, the sac walls seemed solid; however, spheroid cells were scarcely reproduced after sac wall puncturing (Fig. 3D and E). In contrast, spheroid cells were actively reproduced in the case of #25 (Fig. 3F and G). Eventually, the reproduction process persisted up to 60 days after the start of differentiation (data not shown), which was longer than that of hESCs (up to 40 days) (Saeki et al., 2009). Thus, the #25 line bears an equivalent, or even higher, spheroid cell-reproducing potential to hESCs.

We further evaluated the qualities of hematopoietic differentiation of 253G1, 201B7, and #25. First, cytological examinations were performed around day 30 of differentiation, when abundant neutrophil production was observed in the case of hESCs (Saeki et al., 2009). However, vast majorities of the products of 253G1 and 201B7 were macrophages (Fig. 4A, left and middle). On the other hand, various stages of granulocyte-lineage cells, from azurophilc granule-positive myeloid progenitors to segmented granulocytes, were observed in the case of #25 (Fig. 4A, right). Flow cytometric analyses demonstrated that #25-derived spheroid cells were highly positive for CD45, a pan-hematopoietic cell marker, and the majority of cells were positive for CD11b, a granulomonocytic marker (Fig. 4B). To confirm their hematopoietic activities, colony assays were performed (Fig, 4C). The # 25-derived spheroid cells demonstrated equivalent, or even higher, colony-forming unit-granulocyte (CFU-G) ($8.0 \pm 5.3/10^4$ cells; $n = 3$), colony-forming unit-granulocyte/macrophage (CFU-GM) ($12.3 \pm 5.5/10^4$ cells; $n = 3$), colony-forming unit-macrophage (CFU-M) ($21.0 \pm 3.5/10^4$ cells; $n = 3$) to those of hESCs, whose average CFU-G, CFU-GM, and CFU-M per 10^4 cells were 2.3, 7.9, and 3.1, respectively ($n = 2$). Thus, hiPSCs can produce HPCs with equivalent colony-forming activities to hESCs.

We also confirmed the functional maturation of #25-derived neutrophils by performing a superoxide production study (Fig. 5A), a phagocytosis assay (Fig. 5B), and double esterase-staining test (Fig. 5C). Interestingly, the double-esterase staining test, in which neutrophil-specific esterase is stained blue while that of nonspecific monocyte/macrophage esterase is stained brown, demonstrated that #25-derived cells showed even clearer neutrophil-specific blue staining patterns than hESC-derived ones, the majority of which showed brownish blue or bluish brown staining (Fig. 5D). Thus, hiPSCs can generate neutrophil with equivalent, or even higher, maturation levels than hESCs.

For further assessment of possible hematopoietic potentials of 253G1-derived and 201B7-derived spheroid cells, we checked the morphologies of spheroid cells over time. Surprisingly, small round cells with high nucleus/cytoplasm

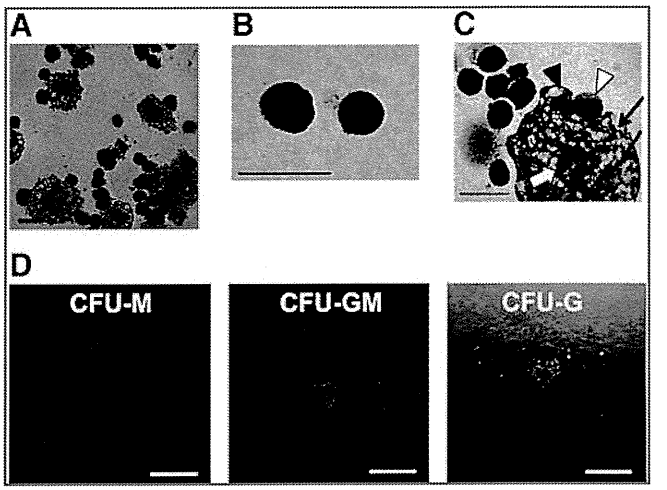

FIG. 6. The hiPCS-derived differentiated cells at early phases. (**A–C**) The 253G1-derived nonadherent cells at day 21 of differentiation were collected and stained by Wright-Giemsa solution. Abundant small cells with particularly high nuclear cytoplasmic ratios were detected (**A, B**). Note that the macrophage contained condensed nucleus-like substances (closed arrow head) and/or chromatin-like substances (arrows) in addition to its own nucleus (open arrow). Small cells were occasionally encompassed by the cytoplasm of macrophages (open arrow head). Scale bars indicate 20 μm. (**D**) The 253G1-derived nonadherent cells at day 23 of differentiation were subjected to colony assays. CFU-M, CFU-GM, and CFU-G were determined by phase contrast microscopic observation. Scale bars indicate 500 μm.

ratios were detected in 253G1-derived samples around day 20 of differentiation (Fig. 6A and B), whereas no such cells were detected in 201B7-derived samples (data not shown). Interestingly, hemophagocytosis-like scenes, where the small cells were phagocytized by macrophages, were often observed (Fig. 6C). Because the morphologies of the small cells resembled to hematopoietic stem/progenitor cells, we checked their colony-forming activities (Fig. 6D). Colony assays performed around day 20 indicated that 253G1-derived cells had comparable CFU-G ($3.3 \pm 2.3/10^4$ cells; $n=3$), CFU-GM ($3.3 \pm 1.2/10^4$ cells; $n=3$), CFU-M ($15.0 \pm 1.0/10^4$ cells; $n=3$) to those of hESCs. On the other hand, few hematopoietic colonies were observed in the case of 201B7 at any time points (data not shown).

Thus, hiPSCs can generate reproducible HPCs with equivalent colony-forming activities to hESC-derived HPCs, although some lines of hiPSCs suffer from defective hematopoietic differentiation.

Discussion

In this article, we have provided the counterexamples to a previously reported finding that hiPSC-derived hemangioblast, the common progenitor of hematopoietic and endothelial cells, suffered from early senescence. In that report, hiPSC-derived HPCs was shown to have substantially decreased colony-forming activities and the majority of hiPSC-derived endothelial cells senesced after one passage (Feng et al., 2010). However, our data have clearly shown that the issue of early senescence can be overcome by selecting appropriate lines of hiPSCs and applying proper differentiation methods to them. Moreover, our results proved that retroviral insertion of reprogramming transgenes was not the cause of early senescence contrary to the discussion by the authors (Feng et al., 2010). We have also shown that, after sequential passages, hiPSC-derived VECs enter senescence as in the cases of hESC-derived VECs and primary human VECs, guaranteeing that hiPSC-derived VECs bear very low tumorigeneity, if any.

The key to our success in producing hiPSC-derived VECs that bear as high growth potentials as hESC-derived counterparts may reside, at least in part, in our usage of multiple hematopoietic cytokines in addition to VEGF. As we have shown previously, the six cytokines, SCF, IL6, IL3, BMP4, Flt3-L, and VEGF, as a whole work for the stable and high-purity production of subculturable VECs (Saeki et al, 2008). Interestingly, we are also observing that, under serum-free conditions, the presence of hematopoietic cytokine cocktail is crucial for the formation of spheres and their subsequent growth on gelatin-coated plates (M.N., unpublished finding). Thus, the usage of hematopoietic cytokine cocktail is advantageous not only for an achievement of high-efficiency differentiation but also survival and proliferation of the differentiated cells. Alternatively, the differentiation process per se, which is often followed by apoptosis, might include antiapoptotic processes as far as the differentiated cells keep surviving. In any event, stressful conditions should be avoided as much as possible from the differentiation procedures of hESCs/hiPSCs as in the case of their maintenance culture, where chromosomal aberrations are reportedly induced via stressful handling of the cells (Draper et al., 2004, Mitalipova et al., 2005).

As we mentioned, two lines of hiPSCs, 253G4 and 201B2, failed in directed differentiation into VECs. The 253G4- and 201B2-derived cells showed poor cord-forming activities and lacked VEC marker expressions, although they possessed Ac-LDL-uptaking capacities and were subculturable over 10 passages (data not shown). Their disadvantageous natures concerning VEC differentiation may be resulted from the possible line dependency in differentiation propensity among hiPSCs as reported in the case of hESCs (Osafune et al., 2008). Indeed, 253G4 and 201B2 showed very poor or no hemaotopoietic differentiation (data not shown). The finding that hiPSC lines with poor VEC-differentiating potentials bear little hemaotocyte-producing capacities seems very reasonable, because hematopoietic cells are derived from a specific population of vascular endothelial cells (Eilken et al., 2009).

Our findings together indicate that, although hiPSCs may be imposed line-dependent limitations in their differentiation capacities, they are not put inevitable fates of differentiation-dependent early senescence.

Acknowledgments

The authors greatly thank Professor Yamanaka at Center for iPS Cell Research and Application, Kyoto University, Japan, for generously providing the hiPSC lines (201B2, 201B7, 253G1, and 253G4). This work was supported by a Grant-in-Aid Scientific Research from the Ministry of Health, Labour and Welfare (KHD1029).

Author Disclosure Statement

The authors declare that no conflicting financial interests exist.

References

Draper, J.S., Smith, K., Gokhale, P., et al. (2004). Recurrent gain of chromosomes 17q and 12 in cultured human embryonic stem cells. Nat. Biotechnol. 22, 53–54.

Eilken, H.M., Nishikawa, S., and Schroeder, T. (2009). Continuous single-cell imaging of blood generation from haemogenic endothelium. Nature 457, 896–900.

Feng, Q., Lu, S.J., Klimanskaya, I., et al. (2010). Hemangioblastic derivatives from human induced pluripotent stem cells exhibit limited expansion and early senescence. Stem Cells 28, 704–712.

Fusaki, N., Ban, H., Nishiyama, A., et al. (2009). Efficient induction of transgene-free human pluripotent stem cells using a vector based on Sendai virus, an RNA virus that does not integrate into the host genome. Proc. Jpn. Acad. Ser. B Phys. Biol. Sci. 85, 348–362.

Kaji, K., Norrby, K., Paca, A., et al. (2009). Virus-free induction of pluripotency and subsequent excision of reprogramming factors. Nature 458, 771–775.

Kim, D., Kim, C.H., Moon, J.I., et al. (2009). Generation of human induced pluripotent stem cells by direct delivery of reprogramming proteins. Cell Stem Cell 4, 472–476.

Mitalipova, M.M., Rao, R.R., Hoyer, D.M., et al. (2005). Preserving the genetic integrity of human embryonic stem cells. Nat. Biotechnol. 23, 19–20.

Miura, K., Okada, Y., Aoi, T., et al. (2009). Variation in the safety of induced pluripotent stem cell lines. Nat. Biotechnol. 27, 743–745.
Nakagawa, M., Koyanagi, M., Tanabe, K., et al. (2008). Generation of induced pluripotent stem cells without Myc from mouse and human fibroblasts. Nat. Biotechnol. 26, 101–106.
Nakagawa, M., Takizawa, N., Narita, M., et al. (2010). Promotion of direct reprogramming by transformation-deficient Myc. Proc. Natl. Acad. Sci. USA 107, 14152–14157.
Nakahara, M., Nakamura, N., Matsuyama, S., et al. (2009). High-efficiency production of subculturable vascular endothelial cells from feeder-free human embryonic stem cells without cell-sorting technique. Cloning Stem Cells 11, 509–522.
Nelson, T.J., Martinez-Fernandez, A., Yamada, S., et al. (2009). Repair of acute myocardial infarction by human stemness factors induced pluripotent stem cells. Circulation 120, 408–416.
Okita, K., Ichisaka, T., and Yamanaka, S. (2007) Generation of germline-competent induced pluripotent stem cells. Nature 448, 313–317.
Okita, K., Nakagawa, M., Hyenjong, H., et al. (2008). Generation of mouse induced pluripotent stem cells without viral vectors. Science 322, 949–953.
Osafune, K., Caron, L., Borowiak, M., et al. (2008). Marked differences in differentiation propensity among human embryonic stem cell lines. Nat. Biotechnol. 26, 313–315.
Saeki, K., Yogiashi, Y., Nakahara, M., et al. (2008). Highly efficient and feeder-free production of subculturable vascular endothelial cells from primate embryonic stem cells. J. Cell Physiol. 217, 261–280.
Saeki, K., Saeki, K., Nakahara, M., et al. (2009). A feeder-free and efficient production of functional neutrophils from human embryonic stem cells. Stem Cells 27, 59–67.
Seki, T., Yuasa, S., Oda, M., et al. (2010). Generation of induced pluripotent stem cells from human terminally differentiated circulating T cells. Cell Stem Cell, 7, 11–14.
Suemori, H., Yasuchika, K., Hasegawa, K., et al. (2006). Efficient establishment of human embryonic stem cell lines and long-term maintenance with stable karyotype by enzymatic bulk passage. Biochem. Biophys. Res. Commun. 345, 926–932.
Takahashi, K., Tanabe, K., Ohnuki, M., et al. (2007). Induction of pluripotent stem cells from adult human fibroblasts by defined factors. Cell 131, 861–872.
Tesar, P.J., Chenoweth, J.G., Brook, F.A., et al. (2007). New cell lines from mouse epiblast share defining features with human embryonic stem cells. Nature 448, 196–199.
Vallier, L., Touboul, T., Chng, Z., et al. (2009). Early cell fate decisions of human embryonic stem cells and mouse epiblast stem cells are controlled by the same signalling pathways. PLoS One 4, e6082.
Warren, L., Manos, P.D., Ahfeldt, T., et al. (2010). Highly efficient reprogramming to pluripotency and directed differentiation of human cells with synthetic modified mRNA. Cell Stem Cell 7, 618–630.
Woltjen, K., Michael, I.P., Mohseni, P., et al. (2009). piggyBac transposition reprograms fibroblasts to induced pluripotent stem cells. Nature 458, 766–770.
Yu, J., Hu, K., Smuga-Otto, K., et al. (2009). Human induced pluripotent stem cells free of vector and transgene sequences. Science 324, 797–801.
Zhou, H., Wu, S., Joo, J.Y., et al. (2009). Generation of induced pluripotent stem cells using recombinant proteins. Cell Stem Cell 4, 381–384.

Address correspondence to:
Kumiko Saeki
Department of Disease Control
Research Institute
National Center for Global Health and Medicine
1-21-1 Toyama Shinjuku-ku
Tokyo 162-8655, Japan

E-mail: saeki@ri.imcj.go.jp

SCIENTIFIC REPORTS

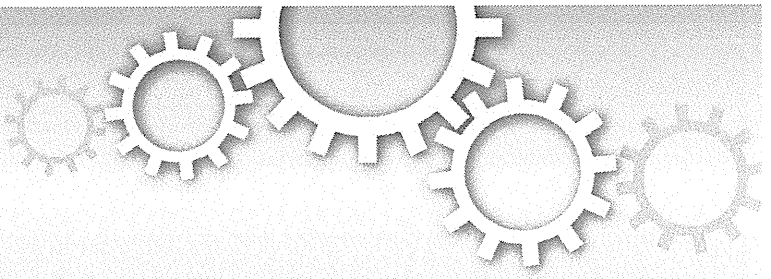

OPEN

SUBJECT AREAS:
BIOLOGICAL SCIENCES
CELL BIOLOGY
MEDICAL RESEARCH
DEVELOPMENTAL BIOLOGY

Received
8 April 2011

Accepted
4 August 2011

Published
19 August 2011

Correspondence and requests for materials should be addressed to K.M. (kmiyado@nch.go.jp)

* These authors equally contributed to this work

β-catenin is a molecular switch that regulates transition of cell-cell adhesion to fusion

Youki Takezawa[1]*, Keiichi Yoshida[1]*, Kenji Miyado[1], Masahiro Sato[2], Akihiro Nakamura[1], Natsuko Kawano[1], Keiichi Sakakibara[1], Takahiko Kondo[1], Yuichirou Harada[1], Naoko Ohnami[1], Seiya Kanai[1], Mami Miyado[1], Hidekazu Saito[3], Yuji Takahashi[3], Hidenori Akutsu[1] & Akihiro Umezawa[1]

[1]Department of Reproductive Biology, National Center for Child Health and Development, 2-10-1 Okura, Setagaya, Tokyo 157-8535, Japan, [2]Section of Gene Expression Regulation, Frontier Science Research Center, Kagoshima University, 1-21-20 Korimoto, Kagoshima, Kagoshima 890-0065, Japan, [3]Division of Reproductive Medicine, Department of Perinatal Medicine and Maternal Care, National Center for Child Health and Development, 2-10-1 Okura, Setagaya, Tokyo 157-8535, Japan.

When a sperm and an oocyte unite upon fertilization, their cell membranes adhere and fuse, but little is known about the factors regulating sperm-oocyte adhesion. Here we explored the role of β-catenin in sperm-oocyte adhesion. Biochemical analysis revealed that E-cadherin and β-catenin formed a complex in oocytes and also in sperm. Sperm-oocyte adhesion was impaired when *β-catenin*-deficient oocytes were inseminated with sperm. Furthermore, expression of β-catenin decreased from the sperm head and the site of an oocyte to which a sperm adheres after completion of sperm-oocyte adhesion. UBE1-41, an inhibitor of ubiquitin-activating enzyme 1, inhibited the degradation of β-catenin, and reduced the fusing ability of wild-type (but not *β-catenin*-deficient) oocytes. These results indicate that β-catenin is not only involved in membrane adhesion, but also in the transition to membrane fusion upon fertilization.

An oocyte fuses to only one sperm at fertilization, which results in the creation of a single cell with two nuclei that undergoes a series of complex processes (Supplementary Fig. S1a)[1]. After the sperm detaches the cumulus cells, the somatic cells surrounding oocytes, from the oocytes by enzymatic activities, the sperm adheres to the zona pellucida (ZP), the oocyte extracellular matrix. The sperm then penetrates the ZP and adheres to the oocyte cell membrane. At this time, fusion occurs between sperm and oocyte.

CD9[2] and Izumo1[3] belong to the tetraspan protein family (tetraspanin) and immunoglobulin superfamily, respectively, and play a crucial role in sperm-oocyte fusion[3–5]. Both *CD9*-deficient oocytes and *Izumo1*-deficient sperm are unable to fuse to their wild-type partner's cells, but retain adhesive activity[3,4]. A couple of these findings suggest that the molecular event underlying membrane adhesion is different from that underlying membrane fusion. The mechanism of membrane fusion has been explored by us[6] and others[7,8], but little is known about the factors regulating the adhesion of a sperm to an oocyte membrane.

Three proteins, β-catenin, α-catenin and E-cadherin, are a well-known functional set mediating intercellular junctions, which are called adherens junctions and typically served as a lateral connector between epithelial cells[9]. Besides epithelial cells, these three proteins are co-expressed in non-epithelial female germ cells, such as immature oocytes and fully-grown oocytes (to which only one sperm can adhere upon fertilization)[10]. Typically, β-catenin directly binds to the cytoplasmic domain of E-cadherin and connects to the adherens junctional complex with actin, a major component of microfilaments[11]. The β-catenin bound to E-cadherin is involved in intercellular adhesion, while E-cadherin-free β-catenin functions as a transcriptional factor driving the Wnt signaling pathway that regulates embryonic morphogenesis[12].

In mouse oocytes, the presence of both β-catenin and E-cadherin has been reported[10], but it remains unclear whether these two proteins are essential during the process of fertilization. In this study, we explored the possible role of β-catenin in sperm-oocyte adhesion, one of the important steps leading to mammalian fertilization.

Results

Subcellular localization of actin and its possible function in sperm-oocyte adhesion. To identify candidate proteins involved in sperm-oocyte membrane adhesion, we first examined immunocytochemically whether two

cytoskeletal proteins, actin and tubulin, would exhibit cortical localization in ovulated oocytes. These two monoclonal antibodies (mAbs) are raised against the conserved domain of actin isoforms or β-tubulin. Confocal microscopic observation demonstrated that actin was asymmetrically localized in the oocyte: namely, metaphase II-arrested chromosomes enclosed by the actin were observed in one side of the oocyte cytoplasm (Supplementary Fig. S1b, c). In addition, actin was found to be concentrated on the cortical surface of the oocyte and appeared to exist as orderly arranged spots beneath the oocyte cell membrane (Supplementary Fig. S1d). Since tetraspanin CD9 is known to be present on the microvilli that regularly line the cell surface of an oocyte[8], oocytes were subjected to double staining with CD9 and actin mAbs. Neither protein was co-localized, and the actin-rich cortical area was clearly separated from the CD9-rich area (Supplementary Fig. S1d, e), implying the presence of at least two types of membranous structures in the oocyte cell membrane, as suggested previously[13]. Since CD9 plays an important role in sperm-oocyte fusion, but not sperm-oocyte adhesion[4], it was hypothesized that the actin-rich membranous structure on the cell surface of an oocyte may be involved in sperm-oocyte membrane 'adhesion'.

E-cadherin/β-catenin complex formation in both oocytes and sperm. Since E-cadherin/β-catenin complex has been known to bind to actin, by which cell-cell membrane adhesion is regulated[9], we considered that this E-cadherin/β-catenin complex may play a role as a regulator of sperm-oocyte membrane adhesion. To assess the problem, we first examined the possible interaction between E-cadherin/β-catenin complex and actin on an oocyte using immunocytochemical methods. In Fig. 1, subcellular localization of α- and β-catenins and E-cadherin is shown and data on the

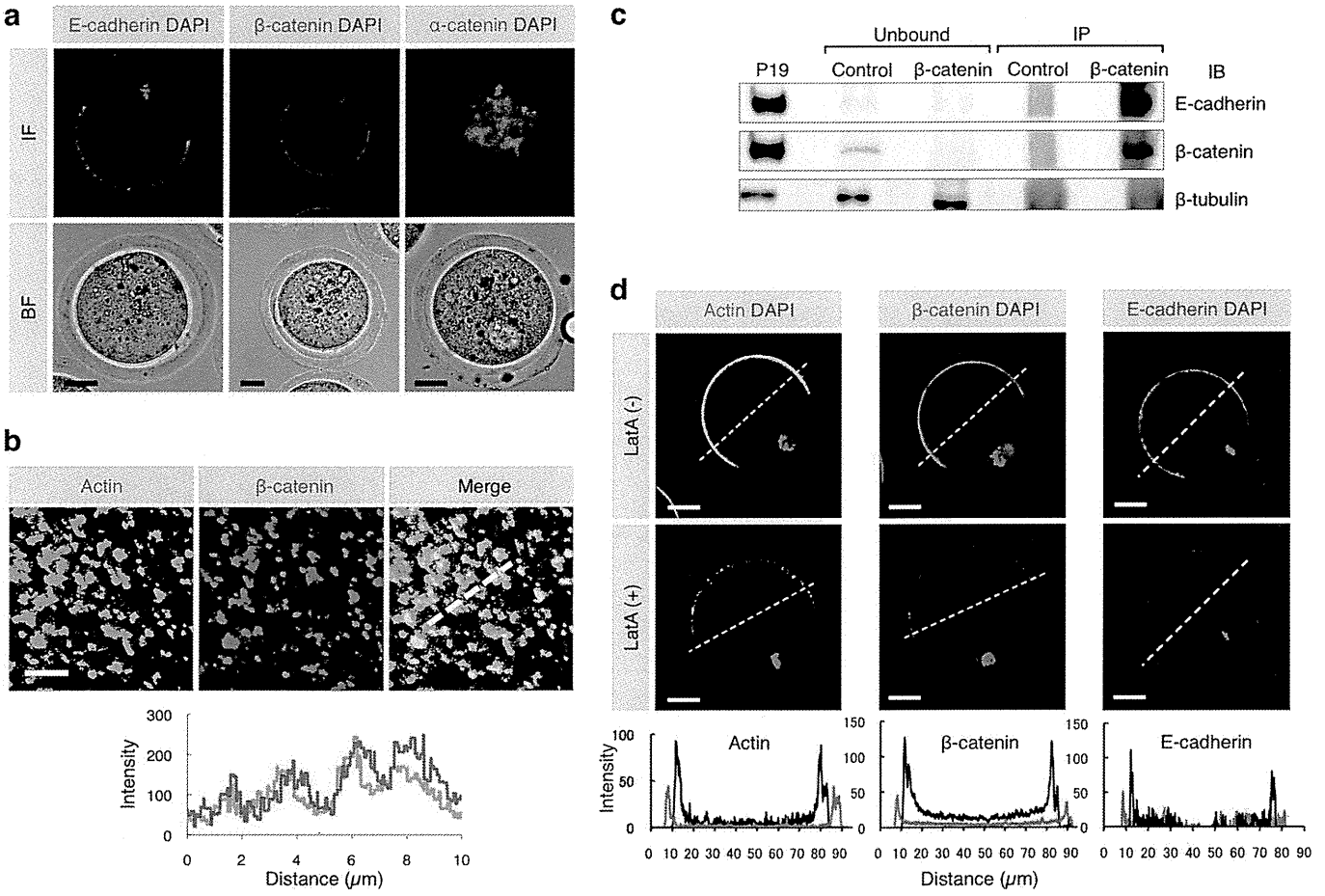

Figure 1 | Expression of E-cadherin and β-catenin and localization of E-cadherin/β-catenin complex in oocytes. (a) Localization of E-cadherin, β-catenin and α-catenin in ovulated oocytes. Similar distribution pattern of E-cadherin and β-catenin on an oocyte suggests complex formation between these two proteins. IF, immunofluorescence; BF, bright field. Scale bars: 20 μm. (b) Localization of β- and γ-actin isoforms and β-catenin beneath the oocyte cell membrane and their fluorescent intensities. The route scanned on the membrane was indicated as a dotted line. Fluorescence intensities for each protein were measured and graphed based on the 3D image, as described in the Experimental Procedures. Red and green lines in the lower panel indicate intensities of β-catenin and actin, respectively. Scale bar: 5 μm. (c) Biochemical evidence for the presence of E-cadherin/β-catenin complex in oocytes. The extract from 905 oocytes immunoprecipitated (IP) by anti-β-catenin mAb and mouse IgG purified from preimmune serum (Control) was subjected to immunoblotting with anti-E-cadherin, anti-β-catenin or anti-β-tubulin mAb. Extracts from mouse embryonic carcinoma cell line P19[35] were also subjected to immunoprecipitation with anti-β-catenin mAb and the resulting immunoprecipitates were reacted with each mAb as a positive control. Note that the extract (IP) immunoprecipitated by anti-anti-β-catenin mAb was reactive with both anti-β-catenin and anti-E-cadherin mAbs, but the extract (Unbound) that was not immunoprecipitated by anti-β-catenin mAb failed to bind to both antibodies. On the other hand, the β-tubulin was detectable in the Ab-unbound (but not Ab-IP) fractions. (d) Disassembly of β-catenin, E-cadherin and actin induced by latrunculin A (latA) treatment. Oocytes were doubly immunostained with anti-β- and γ-actin isoforms mAbs and DAPI (shown as 'Actin DAPI') or with anti-β-catenin mAb or with anti-E-cadherin mAb and DAPI (shown as 'β-catenin DAPI' or 'E-cadherin DAPI'). In the lower panels, the fluorescence intensities measured after being traced along dotted lines in the figures of the upper panels are shown. The intensities of latA-treated oocytes are indicated by red lines, while those of the latA-untreated oocytes are shown by black lines. Scale bar: 20 μm.

comparison between their localization and the localization of actin is also shown. Regarding the immunoreactivity of E-cadherin to an oocyte, a mAb that recognizes an N-terminal extracellular region of E-cadherin was used. Immunocytochemical staining demonstrated that E-cadherin was localized on the cell membrane (microvillar region) of an oocyte that has not been treated with permeabilization (Fig. 1a). β-catenin was detected beneath the oocyte cell membrane, and its localization pattern appeared to be similar to that of E-cadherin (Fig. 1a). In contrast, α-catenin was present in the oocyte cytoplasm (Fig. 1a). When the distribution of β-catenin on an oocyte was compared to that of actin, both proteins were found to be co-localized (Fig. 1b).

Secondly, we assessed the possible formation of β-catenin and E-cadherin complex using an immunoprecipitation method. A cell extract of mouse oocytes (n = 905) was immunoprecipitated with anti-E-cadherin mAb, and the resulting precipitate was then reacted with anti-β-catenin mAb. As a result, the cell extract immunoprecipitated with anti-E-cadherin mAb reacted with the anti-β-catenin mAb (Fig. 1c), indicating the presence of β-catenin and E-cadherin complex in an oocyte.

Thirdly, we assessed the effect of latrunculin A (latA), an inhibitor of actin polymerization, on the formation of β-catenin and E-cadherin complex. When oocytes were treated with 10 μM latA for 1 h at 37°C, actin immunoreactivity was reduced along with decreased immunoreactivity to β-catenin and E-cadherin (Fig. 1d). These results suggest that the β-catenin/E-cadherin complex formed in the oocyte cell membrane is closely associated with actin.

Since the β-catenin/E-cadherin complex is known to play a role in cell-cell adhesion via its homophilic interaction with E-cadherin[14], we predicted that this protein complex would also be produced in sperm. To test this hypothesis, epididymal capacitated sperm were collected from 10-week-old males and subjected to Western blotting (Fig. 2a) and immunoprecipitation (Fig. 2b) analyses. Western blotting revealed that both E-cadherin and β-catenin were detected in the sperm collected (Fig. 2a); however, N-cadherin was not detectable in those samples (Fig. 2a), although its expression has been reported in mouse oocytes[15]. Immunoprecipitation analysis also revealed the presence of the E-cadherin/β-catenin complex in sperm. The sperm extracts immunoprecipitated with anti-β-catenin mAb were reactive with anti-E-cadherin mAb, and those immunoprecipitated with anti-E-cadherin mAb were reactive with anti-β-catenin mAb (Fig. 2b). To confirm this further, immunocytochemical staining was performed for the isolated sperm. Staining of unpermeabilized sperm with anti-E-cadherin mAb demonstrated that E-cadherin was broadly expressed on the cell membrane of sperm from the head region to the mid-piece as well as part of the tail (Fig. 2c, d). Staining of permeabilized sperm with anti-β-catenin mAb revealed that the expression of β-catenin was localized beneath the sperm cell membrane and, notably, its localization pattern was similar to that of E-cadherin (Fig. 2c, d).

In mammals, both sperm-oocyte fusion and adhesion have been believed to occur in a specific region of the sperm head, called an equatorial segment (ES)[1]. Therefore, it is reasonable to consider that factor(s) regulating sperm-oocyte adhesion should exist in this segment. Since in the sperm head of the Asian musk shrew, *Suncus murinus*, ES is recessed within the waist of the sperm nucleus[16], it is easy to detect proteins localized in this segment. When immunocytochemical staining of the permeabilized shrew capacitated sperm was performed using anti-E-cadherin mAb, E-cadherin was expressed on the ES, the mid-piece and part of the tail (Supplementary Fig. S2a). Staining with anti-β-catenin mAb revealed the expression of β-catenin specifically localized on the ES of the sperm head (Supplementary Fig. S2b). Notably, its localization pattern was similar to that of E-cadherin in the shrew sperm (Supplementary Fig. S2a *vs.* Fig. S2b) and also to that of E-cadherin in the mouse sperm (Fig. 2c, d). Furthermore, some β-catenin molecules were released from the acrosomes of the shrew sperm (Supplementary Fig. S2b). Since the ES is recessed in the acrosome of the shrew sperm[16], β-catenin may have accumulated specifically in the ES upon completion of ES formation. These collected results led to a conclusion

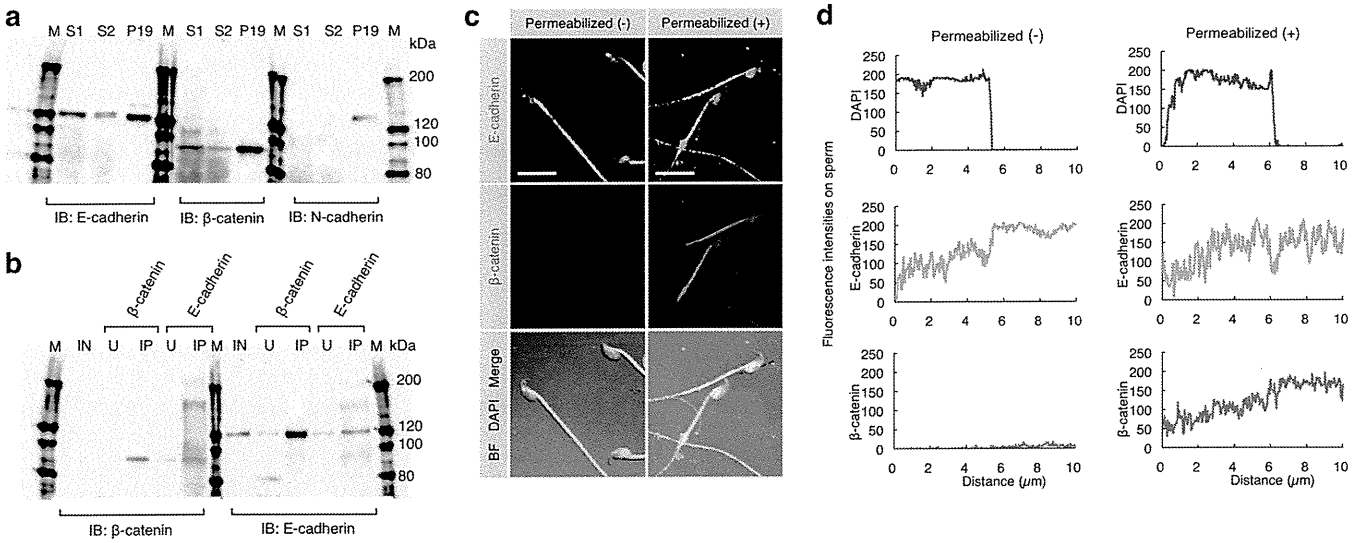

Figure 2 | Expression of E-cadherin and β-catenin and their interaction in sperm. (a) Expression of E-cadherin and β-catenin in epididymal sperm. E-cadherin and β-catenin, but not N-cadherin, in the sperm were detected by immunoblotting (IB). Sperm (S1 and S2) were collected from the epididymis of two males and used for IB. Extracts from P19 cells were used as a positive control. IB was performed using anti-E-cadherin, anti-β-catenin or anti-N-cadherin mAbs. M, molecular weight markers. (b) Interaction between E-cadherin and β-catenin in sperm. Extracts from the sperm (used as input sample (IN)) were immunoprecipitated by anti-E-cadherin or anti-β-catenin mAb. The precipitates (IP) and unbound extracts (U) were immunoblotted (IB) with anti-E-cadherin or anti-β-catenin mAb. M, molecular weight markers. (c) Localization of E-cadherin and β-catenin in sperm. Unpermeabilized or permeabilized sperm were doubly immunostained with anti-E-cadherin (ECCD-2) and anti-β-catenin mAbs, and their nuclei were stained with DAPI. ECCD-2, which recognizes an epitope in the N-terminal extracellular region of E-cadherin, bound to E-cadherin without permeabilization pretreatment. Scale bar: 5 μm. (d) The fluorescence intensity profiles of E-cadherin and β-catenin in sperm shown in (c). Fluorescence intensities were measured after being traced on the sperm along dotted lines shown at the bottom of the panels in (c).

that mammalian epididymal sperm always form E-cadherin/β-catenin complex.

Generation of *β-catenin*-, *α-catenin*- and *E-cadherin*-deficient oocytes. To determine which genes are involved in sperm-oocyte adhesion among *β-catenin*, *α-catenin* and *E-cadherin* genes, three strains (*E-cadherin*$^{floxed/floxed}$ [17], *β-catenin*$^{floxed/floxed}$ [18], and *α-catenin*$^{floxed/floxed}$ [19]) with *loxP*-flanked genes were inter-crossed with the transgenic mouse strain (*Tg*$^{ZP3\text{-}cre/+}$) expressing cre-recombinase in an oocyte-specific manner. Offspring (F2) lacking each type of gene (*E-cadherin*$^{floxed/floxed}$*Tg*$^{ZP3\text{-}cre/+}$, *β-catenin*$^{floxed/floxed}$*Tg*$^{ZP3\text{-}cre/+}$ and *α-catenin*$^{floxed/floxed}$*Tg*$^{ZP3\text{-}cre/+}$) were successfully obtained according to the Menderian inheritance rule (see Methods; Supplementary Fig. S3a), and were all viable and normal in size without displaying any overt physical or behavioral abnormalities. When the number of ovulated oocytes from these superovulated offspring was counted and compared with that of oocytes from the control floxed mice, there were no clear differences in the number of ovulated oocytes between the two groups: 11.7 ± 1.4 (n = 25) for *E-cadherin*$^{floxed/floxed}$*Tg*$^{ZP3\text{-}cre/+}$and 13.7 ± 1.9 (n = 22) for *E-cadherin*$^{floxed/floxed}$; 23.2 ± 1.5 (n = 21) for *β-catenin*$^{floxed/floxed}$*Tg*$^{ZP3\text{-}cre/+}$ and 23.2 ± 1.5 (n = 19) for *β-catenin*$^{floxed/floxed}$; 15.6 ± 2.4 (n = 9) for *α-catenin*$^{floxed/floxed}$*Tg*$^{ZP3\text{-}cre/+}$ and 12.4 ± 2.3 (n = 9) for *α-catenin*$^{floxed/floxed}$. Oocytes isolated from each line carrying the *cre-recombinase* gene were not morphologically distinguishable from those from each control floxed line (Supplementary Fig. S3b). To confirm whether oocytes from these gene-disrupted mice exhibit loss of target protein expression, oocytes were subjected to immunocytochemical staining together with oocytes from control floxed mice. E-cadherin, β-catenin and α-catenin were indeed absent from oocytes of *E-cadherin*$^{floxed/floxed}$*Tg*$^{ZP3\text{-}cre/+}$, *β-catenin*$^{floxed/floxed}$*Tg*$^{ZP3\text{-}cre/+}$ and *α-catenin*$^{floxed/floxed}$*Tg*$^{ZP3\text{-}cre/+}$, respectively (Supplementary Fig. S3b). These results suggest that these three genes are not essential for the maturation and ovulation of mouse oocytes.

In epithelial cells, β-catenin is required for localization of E-cadherin on the cell surface, and endocytosis of E-cadherin into the cytoplasm occurs in the absence of β-catenin[20]. In addition, a model was proposed: α-catenin participates to bind to the E-cadherin/β-catenin complex to connect with actin microfilaments under certain specific conditions[9]. In analogy to this, it is possible that cellular localization of E-cadherin, β-catenin and α-catenin is mutually regulated in oocytes. Such a possibility is already depicted in Fig. 1a, in which E-cadherin was co-localized with β-catenin, but not with α-catenin on a wild-type oocyte. To examine whether the formation of E-cadherin/β-catenin complex (possibly E-cadherin/β-catenin/α-catenin complex) is impaired when either one of these composite proteins is deficient, oocytes collected from all of the gene-ablated strains were immunocytochemically assessed for localization of these three proteins (Supplementary Fig. S4a–c). Expression of E-cadherin was strongly reduced on the cell membrane of *β-catenin*-deficient oocytes, but not *α-catenin*-deficient oocytes (Supplementary Fig. S4a *vs.* Fig. S4b). On the other hand, loss of E-cadherin did not affect the localization pattern of β-catenin and α-catenin (Supplementary Fig. S4c). Similar results were also obtained when *α-catenin*-deficient oocytes were examined (Supplementary Fig. S4a). These results indicate that β-catenin regulates the membrane localization of E-cadherin in mouse oocytes.

Sperm-oocyte adhesion or fusion assay. Membrane interaction between oocytes and sperm occurs after the penetration of sperm into ZP (Supplementary Fig. S1a). To monitor such interaction directly, 'ZP-free' *β-catenin*-deficient oocytes after enzymatic digestion of ZP were inseminated with wild-type epididymal sperm (Fig. 3a, b for adhesion assay; Fig. 3c–e for fusion assay). 'ZP-free' oocytes from *β-catenin*$^{floxed/floxed}$ mice were used as a control. When the oocytes were inspected 1 h after insemination and stained with 4',6-diamidino-2-phenylindole (DAPI) after fixation, as depicted in Fig. 3a, the number of sperm adhered to 'ZP-free' *β-catenin*-deficient oocytes was significantly reduced (Fig. 3b) compared to sperm bound to control oocytes. Similarly, when DAPI-preloaded oocytes were inspected 1 h after insemination, as depicted in Fig. 3c, the relative rate of 'ZP-free' *β-catenin*-deficient oocytes fused with sperm was also significantly reduced (39.2 ± 12.7 *vs.* 100.0 for control oocytes; $P<0.003$; Fig. 3d, e). We next examined the expression pattern of CD9, an essential protein for fusion[4], in *β-catenin*-deficient oocytes immunocytochemically and immunobiochemically to assess the ability of wild-type C57BL/6N sperm to fuse with their membrane. CD9 was expressed on the plasma membrane of 'ZP-free' *β-catenin*-deficient oocytes at a level comparable to that of 'ZP-free' control oocytes (Supplementary Fig. S5a). The total amount of CD9 quantified by immunoblotting in *β-catenin*-deficient oocytes was comparable to that of control oocytes (Supplementary Fig. S5b). These findings suggest that β-catenin is involved in sperm-oocyte adhesion.

***In vitro* fertilizing ability of *β-catenin*-deficient oocytes.** To know how fertilization is influenced by the dysfunction of sperm-oocyte adhesion, we determined the fertilization rate of *β-catenin*-deficient oocytes. The *β-catenin*-deficient oocytes surrounded by cumulus cells (herein referred to as 'cumulus-intact' oocytes) were isolated from oviducts and directly subjected to IVF with wild-type sperm, as depicted in Fig. 3f. 'Cumulus-intact' oocytes from *β-catenin*$^{floxed/floxed}$ mice were used as a control. When the oocytes were inspected 24 h after insemination, the relative rate of *β-catenin*-deficient oocytes fused with sperm was not reduced (Fig. 3g). Quantitative analysis revealed that the rate of *β-catenin*-deficient oocytes fused with sperm was rather enhanced (119.6 ± 4.6 *vs.* 100.0 for control oocytes; $P<0.02$; Fig. 3h), in contrast with the results of the previous adhesion/fusion assay (Fig. 3a–e). This is probably due to the occasional presence of the oocytes fused to sperm, which failed to develop to the two-cell stage; however, the fact that certain embryos developed to the two-cell stage would not exclude the possibility of pathogenetic activation of oocytes. On the other hand, the IVF rate (which is evaluated by the development of fertilized oocytes to the two-cell stage) was comparable between the two groups (Fig. 3i).

We further confirmed the above point by counting litters obtained through mating between *β-catenin*$^{floxed/floxed}$*Tg*$^{ZP3\text{-}cre/+}$ females and *β-catenin*$^{floxed/floxed}$ males. The control *β-catenin*$^{floxed/floxed}$ females were similarly mated. The litter size of *β-catenin*$^{floxed/floxed}$*Tg*$^{ZP3\text{-}cre/+}$ females was 5.3 ± 0.4, which was comparable with that of control females (5.8 ± 0.4) (Supplementary Fig. S6). These results indicate that oocytes lacking β-catenin expression reduce the ability to adhere with sperm, but sustain the ability to fuse with sperm as well as the total reproductive ability needed for delivering pups.

Possible involvement of β-catenin in transition of membrane adhesion to fusion. To examine the dynamics of β-catenin at sperm-oocyte membrane adhesion, alteration in the localization pattern of β-catenin at the sperm attachment sites of the *in vitro* fertilized "zona-free" oocyte was monitored (Fig. 4a–c). Before sperm attachment, β-catenin-rich patches (as shown in Fig. 1b) were clearly detected on the surface of an oocyte (upper left panel of Fig. 4a); however, these patches became undetectable 30 min after sperm attachment (arrows in the lower left panel; Fig. 4a). Furthermore, β-catenin was abundantly present in the capacitated sperm head (upper middle and right panels of Fig. 4a) before sperm attachment, but the amount of β-catenin in sperm heads was also greatly reduced after insemination (arrows in the lower middle and right panels; Fig. 4a). In addition, β-catenin was localized in the sperm head, although its localization pattern was slightly different in each sperm. Notably, β-catenin tended to be concentrated at ES (Fig. 2c; Supplementary Fig. S2; Fig. 4a).

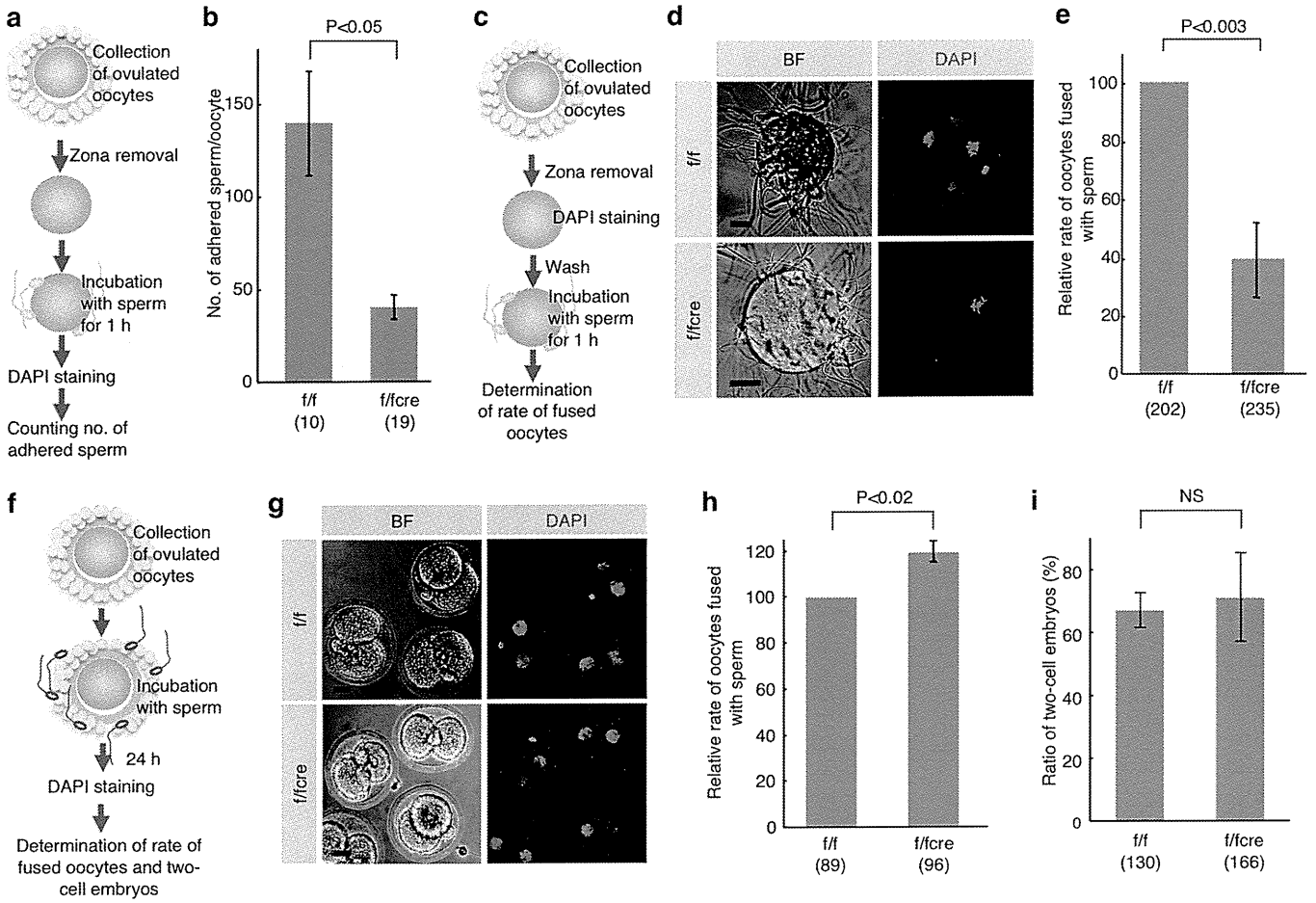

Figure 3 | *In vitro* fertilizing ability of *β-catenin*-deficient oocytes. (a) Experimental flow for testing sperm-oocyte membrane 'adhesion', and comparison of the number of wild-type sperm adhered to an 'zona-free' oocyte between f/fcre and f/f oocytes. After ZP removal, 'zona-free' oocytes were mixed with sperm for 1 h. (b) The number of sperm adhered to an oocyte was counted by DAPI-derived fluorescence in sperm heads on the surface of an oocyte. Parentheses indicate the number of oocytes examined. Values are the mean ± standard error (SE). (c) Experimental flow for testing sperm-oocyte membrane 'fusion' and fused sperm (shown as DAPI-positive sperm) in 'zona-free' *β-catenin*-deficient (f/fcre) and control (f/f) oocytes. After ZP removal, subsequent preincubation for 20 min in the presence of DAPI and washing, 'zona-free' oocytes were mixed with the wild-type sperm for 1 h. (d) Comparison of oocytes fused with sperm between f/fcre and f/f oocytes. BF, bright field. Bars: 20 μm. (e) Comparison of the relative rate of oocytes fused with sperm between f/fcre and f/f oocytes. Only oocytes having at least one fused sperm were counted. The comparative values relative to the control (f/f oocytes; set to 100.0) were displayed as the relative rate of fused oocytes. Parentheses indicate the number of oocytes examined in triplicate experiments. Values are the mean ± SE. (f) Experimental flow for testing sperm-oocyte membrane interaction and fused sperm in two-cell embryos developing from 'cumulus-intact' *β-catenin*-deficient (f/fcre) and control (f/f) oocytes. DAPI staining was performed to detect fused sperm on the developing two-cell embryos. (g) Comparison of oocytes fused with sperm between "cumulus-intact" f/fcre and f/f oocytes. Bars: 20 μm. (h) Comparison of the relative rate of oocytes fused with sperm between "cumulus-intact" f/fcre and f/f oocytes. Parentheses indicate the number of oocytes examined in triplicate experiments. Values are the mean ± SE. (i) Comparison of the ratio of oocytes developing to two-cell stage 24 h after fertilization between "cumulus-intact" f/fcre and f/f oocytes, according to the procedure described in (f). Parentheses indicate the total number of oocytes examined in triplicate experiments. NS, not significant. Values are the mean ± SE.

These findings could also be supported by measurement of fluorescent intensities of β-catenin (Fig. 4b, c). When fluorescence intensity at the equator of an oocyte (dotted line in the upper image of the left panels; Fig. 4a) was compared with that in the region of an oocyte adhered to sperm (dotted line in the lower image of the left panels; Fig. 4a), intense localization of β-catenin in the oocyte exhibiting no sperm attachment was observed beneath the oocyte membrane (arrows in the upper graph; Fig. 4b); however, 30 min after sperm attachment, the fluorescent intensity of β-catenin beneath the oocyte membrane was markedly reduced (arrows in the lower graph; Fig. 4b). Concomitantly, fluorescence intensity throughout the entire sperm (dotted lines in the right panels; Fig. 4a) was quantitatively compared before and after sperm adhesion to the oocyte membrane (Fig. 4c). Before attachment to the oocyte membrane, β-catenin was broadly localized in the sperm head (corresponding to the DAPI-stained region), mid-piece and part of the tail (Fig. 2c, d; upper graph of Fig. 4c); however, after attachment to the oocyte membrane, the intensity of β-catenin in the sperm head (but not in a mid-piece and tail) was markedly decreased (arrows in the lower middle and right panels of Fig. 4a; lower graph of Fig. 4c). Moreover, to confirm that the amount of β-catenin is reduced at steps between sperm-oocyte adhesion and fusion, localization pattern of β-catenin at the sperm attachment sites of the *in vitro* fertilized "zona-free" *CD9*-deficient oocyte was monitored (Fig. 4d, e). Before sperm attachment, intense localization of β-catenin (as shown in the upper left panel of Fig. 4a) was clearly seen on the surface of an oocyte (upper middle panel of Fig. 4d); however, these patches became undetectable 30 min after sperm attachment (arrows in the lower middle panel; Fig. 4d). These findings were also confirmed by measurement of fluorescent intensities of β-catenin (Fig. 4e). When

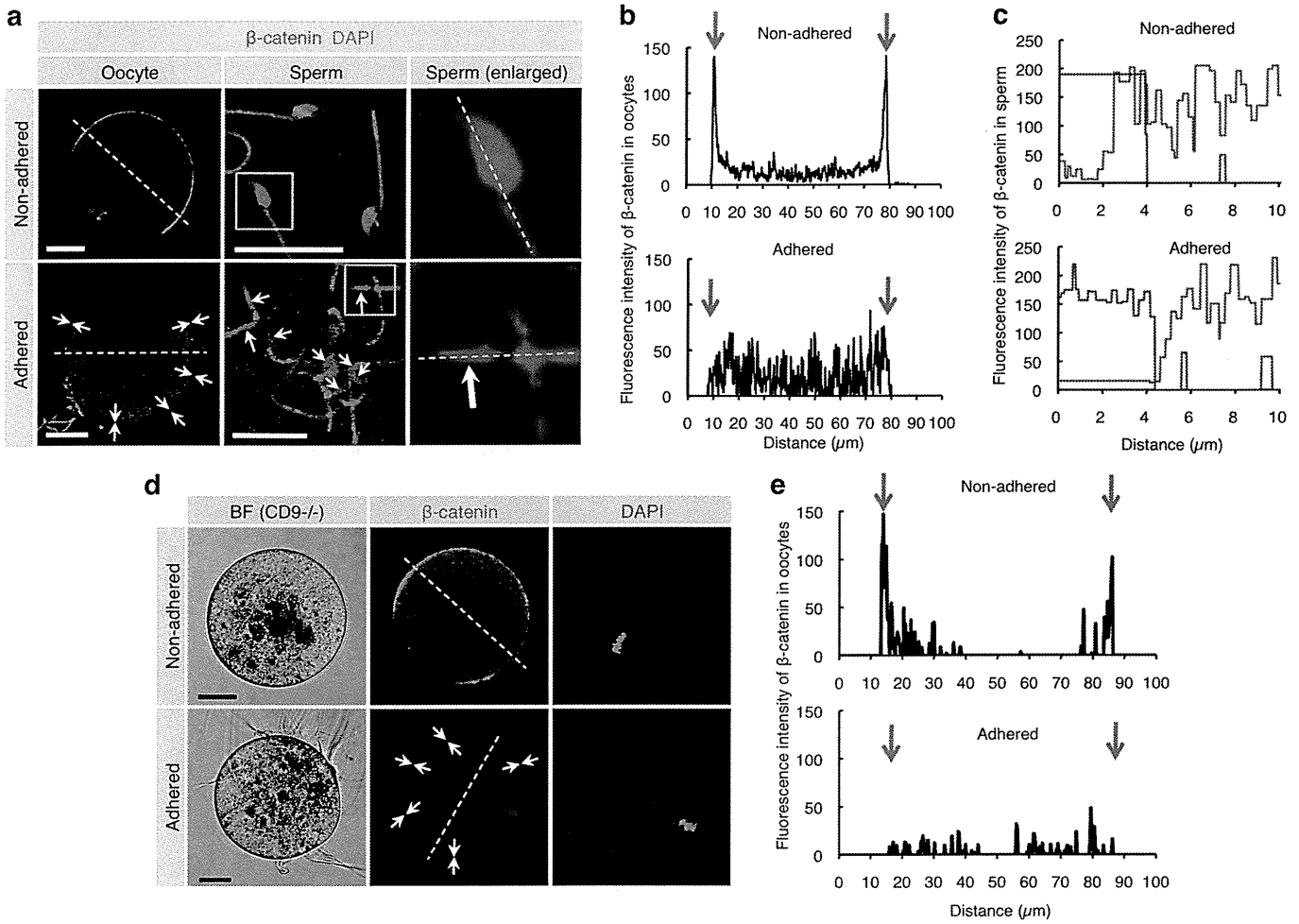

Figure 4 | Reduced levels of β-catenin localized beneath the cell membrane of both oocytes and sperm after membrane adhesion. (a) β-catenin disassembly induced by membrane adhesion in oocytes and sperm. In the 'Non-adhered' group (upper panels), ZP-denuded C57BL/6N oocytes were stained with DAPI and subsequently reacted with anti-β-catenin mAb. Also, epididymal sperm were stained with DAPI and anti-β-catenin mAb. In the 'Adhered' group (lower panels), ZP-denuded C57BL/6N oocytes were stained with DAPI and then subjected to IVF for 30 min prior to incubation with anti-β-catenin mAb. Arrows indicate areas where fluorescent intensities of β-catenin are reduced. In each panel, boxes in middle sets of panels were enlarged and shown on the right. Scale bars: 20 and 10 μm in left and middle panels, respectively. (b) Fluorescence intensities of oocytes before and after sperm-oocyte adhesion. Fluorescence intensities were measured after being traced along dotted lines in the left panels of (a). Arrows indicate both sides of the oocyte cell membranes. (c) Fluorescence intensities of sperm before and after sperm-oocyte adhesion. Fluorescence intensities were measured after being traced along dotted lines in the right panels of a. Red and blue lines indicate fluorescent intensities for β-catenin and DAPI, respectively. (d) β-Catenin disassembly induced by membrane adhesion in oocytes and sperm. In the 'Non-adhered' group (upper panels), ZP-denuded *CD9-/-* oocytes were stained with DAPI and subsequently reacted with anti-β-catenin mAb. In the 'Adhered' group (lower panels), ZP-denuded *CD9-/-* oocytes were preloaded with DAPI as depicted in Fig. 3c and then subjected to IVF for 30 min prior to incubation with anti-β-catenin mAb. Arrows indicate areas where fluorescent intensities of β-catenin are reduced. In each panel, Scale bars: 20 μm. (e) Fluorescence intensities of *CD9-/-* oocytes before and after sperm-oocyte adhesion. Fluorescence intensities were measured after being traced along dotted lines in the left panels of d. Arrows indicate both sides of the oocyte cell membranes.

fluorescence intensity at the equator of an oocyte (dotted line in the upper image of the middle panel; Fig. 4d) was compared with that in the region of an oocyte adhered to sperm (dotted line in the lower image of the middle panel; Fig. 4d), intense localization of β-catenin in the oocyte exhibiting no sperm attachment was observed beneath the oocyte membrane (arrows in the upper graph; Fig. 4e); however, 30 min after sperm attachment, the fluorescent intensity of β-catenin beneath the oocyte membrane was markedly reduced (arrows in the lower graph; Fig. 4e). These collective data imply that alteration in the localization of β-catenin in both sperm and oocyte membranes may contribute to the transition of cell adhesion to fusion.

Generally, in the absence of Wnt signal, E-cadherin-free cytoplasmic β-catenin is rapidly degraded due to "ubiquitination", while only membrane-anchored β-catenin, which is associated with E-cadherin, is resistant to such degradation[21]. Since the fluorescence intensity of β-catenin beneath cell membranes was greatly reduced in both sperm and oocytes after membrane adhesion, ubiquitination may be involved in such reduction. In other words, degradation of β-catenin may be involved in the transition from adhesion to fusion upon sperm-oocyte interaction. To test this possibility, we employed an inhibitor of the ubiquitination pathway to investigate whether it can disturb sperm-oocyte fusion. UBE1-41, a specific inhibitor of ubiquitin-activating enzyme 1 (UBE1), is known to impair antigen-induced FcεRI ubiquitination and internalization[22] and to inhibit melanocortin-4 receptor internalization via ubiquitination[23]. To determine the optimal concentration of UBE1-41, we first assessed sperm-oocyte interaction by co-incubation of sperm and

oocytes in TYH medium containing various amounts of UBE1-41 (0, 1, 5, 10, 20 or 50 μM). We finally decided to use 10 μM UBE1-41, because treatment with more than 20 μM UBE1-41 caused deleterious effects on oocytes. Notably, this concentration (10 μM) appears to be lower than that (50 μM) reported previously[22]. "Zona-free" oocytes treated with 10 μM UBE1-41 for 30 min were incubated with sperm and the ratio of fused oocytes was measured (Fig. 5a). As depicted in Fig. 4a, c, the fluorescence intensity of β-catenin beneath cell membranes was greatly reduced in the untreated oocyte after membrane adhesion with sperm (arrows in the upper left panel; Fig. 5b); however, intense localization of β-catenin was observed beneath the oocyte membrane in the oocyte treated with UBE1-41 even after membrane adhesion with sperm (arrows in the lower left panel; Fig. 5b), and β-catenin-rich patches (oocyte before membrane adhesion; Fig. 1b) were clearly detected on the surface of the oocyte (lower right panel; Fig. 5b). The rate of oocyte fusion with sperm was inversely correlated with the intense localization of β-catenin beneath the cell membrane: treatment with UBE1-41 lowered the rate of fused oocytes in contrast with that of untreated oocytes (51.7 ± 6.2 for UBE1-41-treated oocytes *vs.* 100.0 for untreated oocytes; $P<0.0001$; Fig. 5c; Supplementary Fig. S7). This result suggests that β-catenin ubiquitination leading to degradation is involved in transition from membrane adhesion to fusion. Given this background, it seems likely that the loss of β-catenin facilitates sperm-oocyte fusion. In other words, the fusing ability of *β-catenin*-deficient oocytes should be unaffected by treatment with UBE1-41. In fact, *β-catenin*-deficient oocytes exhibited fusing ability, although they were unable to adhere to sperm (Fig. 3). Furthermore, treatment of *β-catenin*$^{floxed/floxed}$*Tg*$^{ZP3\text{-}cre/+}$ oocytes with UBE1-41 did not affect the rate of fused oocytes (90.6 ± 11.3 for UBE1-4-treated oocytes *vs.* 100.0 for untreated oocytes; Fig. 5d). By contrast, similar treatment of *β-catenin*$^{floxed/floxed}$ oocytes resulted in reduction of their fusing ability, as expected (55.3 ± 11.5 for UBE1-4-treated oocytes *vs.* 100.0 for untreated oocytes; $P<0.02$; Fig. 5d). These results led us

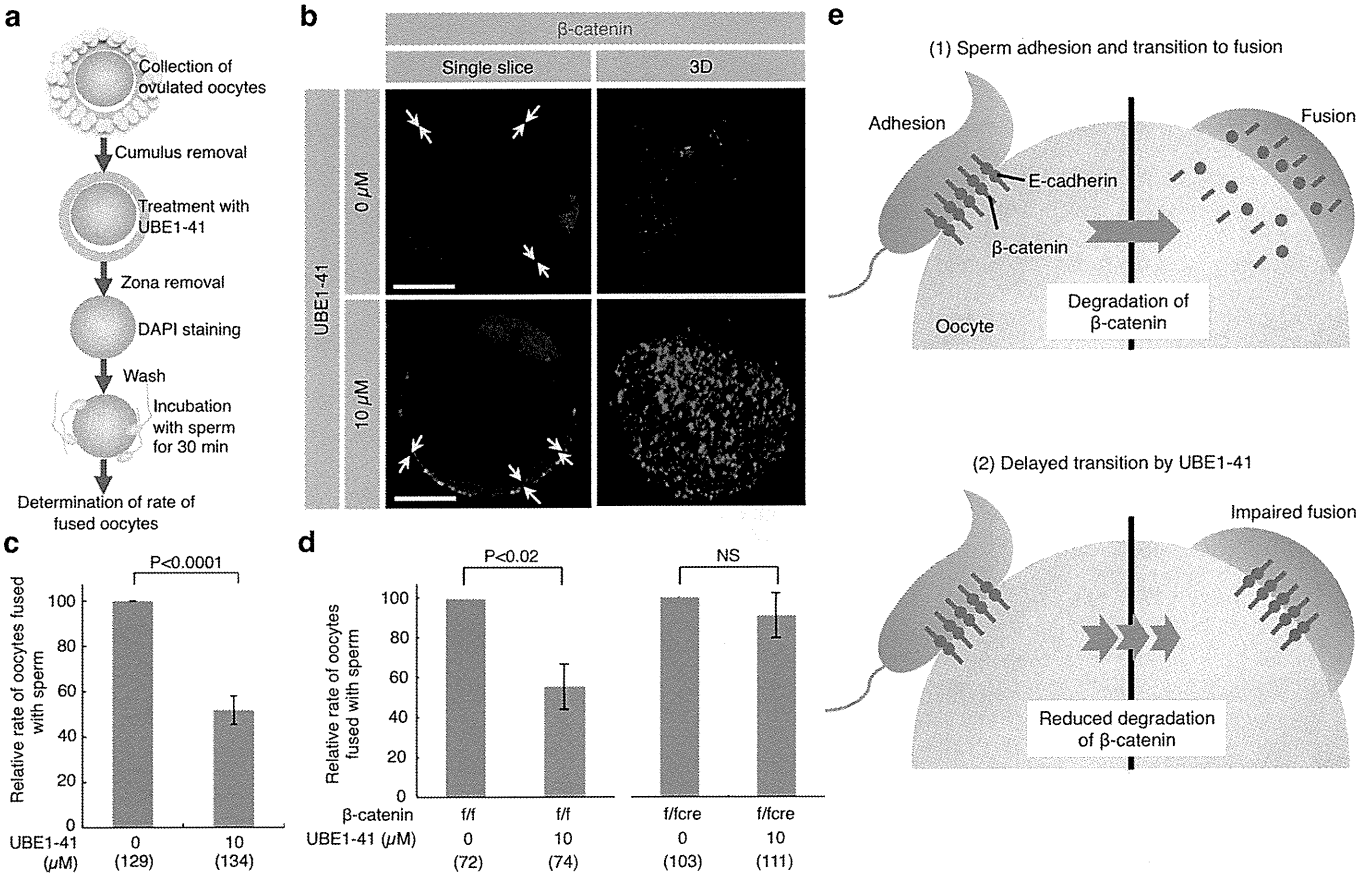

Figure 5 | Reduced fusing ability of oocytes treated with UBE1-41, an inhibitor of ubiquitination. (a) Experimental flow. Cumulus cells attached to the oocytes collected from oviducts were removed. The oocytes were then treated with UBE1-41 for 30 min, followed by ZP removal. After 20-min incubation with DAPI-containing medium and subsequent washing, 'zona-free' oocytes were mixed with the sperm and incubated for 30 min. Only oocytes having at least one fused sperm were counted as fused oocytes. (b) Sustained expression of β-catenin on the surface of "zona-free" wild-type oocytes treated with UBE1-41 after membrane adhesion with sperm. Arrows indicate oocyte cell membranes where β-catenin deposition is noted. One sperm fused with the untreated oocyte (upper panel), but not with the UBE1-41-treated oocyte (lower panel). To focus on the β-catenin expression, only fluorescent images are shown. Single slice, Image captured when the diameter of an oocyte was longest; 3D, 3-dimensional image reconstructed from serial scanned images. Bars: 20 μm. (c) Decreased number of fused sperm on "zona-free" wild-type oocytes after treatment with UBE1-41. The relative rate of oocytes carrying fused sperm was compared between UBE1-41-treated and -untreated wild-type oocytes. The comparative values relative to the control (set to 100.0) are displayed as the relative rate of fused oocytes. As described in the legend of Fig. 3c, oocytes fused with sperm are defined as those with at least one DAPI-positive sperm. (d) Comparison of the relative rate of oocytes carrying fused sperm between UBE1-41-treated and untreated oocytes (*β-catenin*-deficient (f/fcre) *vs. β-catenin*-intact (f/f) oocytes). Comparison was made as described in (c). NS, not significant. Parentheses indicate the total number of oocytes examined in triplicate experiments. Values are the mean ± SE. (e) A model of the possible role of β-catenin in transition from membrane adhesion to fusion. At fertilization (as described in (1)), adhesion of sperm to the surface of an oocyte is mediated by E-cadherin/β-catenin complex; however, subsequent fusion requires rapid degradation of β-catenin. On the other hand, in the presence of UBE1-41 (as described in (2)), adhesion occurs normally, but fusion is impaired since UBE1-41 inhibits degradation of β-catenin.

to consider that β-catenin may be accumulated around sperm attachment sites through the formation of a protein complex with E-cadherin, but immediately diminished when sperm-oocyte fusion occurred. This transient formation of such complex encouraged us to suppose that the E-cadherin/β-catenin complex plays an important role in the transition from membrane adhesion to membrane fusion during sperm-oocyte interaction (Fig. 5e).

Discussion

Membrane fusion occurs after membrane adhesion. Such a process is also true for sperm-oocyte interaction[1]. Our present results indicate that both E-cadherin and β-catenin are involved in sperm-oocyte membrane adhesion. This is demonstrated by the fact that *β-catenin*-deficient oocytes can fuse to sperm, and develop normally to term.

E-cadherin is involved in homophilic adhesion between epithelial cells, and transduces external signaling via α-catenin and β-catenin[9]. In contrast, E-cadherin remains essential for basic cell-cell adhesion, even in the absence of α-catenin, in human prostate carcinoma PC3 cells[24], suggesting that the formation of E-cadherin/β-catenin/actin microfilament complex is proceeded by other molecule(s) in the absence of α-catenin. In analogy, at sperm-oocyte adhesion, association between the E-cadherin/β-catenin complex and actin microfilaments may be mediated by molecule(s) other than α-catenin or the E-cadherin/β-catenin complex itself can directly bind to actin microfilaments, although evidence for this remains to be provided.

Rapid reduction in the level of β-catenin occurs after increased ubiquitination and degradation through a proteosomal pathway[21]. N-Acetyl-Leu-Leu-Nle-CHO (ALLN), a specific inhibitor of the proteolytic activity of proteasomes is reported to inhibit sperm-oocyte fusion upon fertilization[25], implying that the ubiquitination-proteasome pathway may play a role in sperm-oocyte interaction by regulating the quantity of β-catenin on sperm and oocyte membranes. Giving that β-catenin is present on the sperm head and oocyte surface, and that its elimination impairs sperm-oocyte adhesion (see Fig. 3b), it is conceivable that the ubiquitination-proteasome pathway is a key that mediates phase transition from membrane adhesion to fusion, as genetic studies in *C. elegans* have identified multiple roles for the ubiquitin system in early development[26].

Taken together, our results propose a model regarding the transition from membrane adhesion to fusion upon sperm-oocyte interaction (Fig. 5e). Before sperm-oocyte adhesion, both sperm and oocyte retain the β-catenin/E-cadherin complex, a complex important for sperm-oocyte adhesion. Once sperm-oocyte adhesion occurs, β-catenin is immediately ubiquitinated and probably degraded in both the sperm and oocyte, thereby initiating membrane fusion between these two cells; however, in oocytes treated with UBE1-41, ubiquitination of β-catenin associated with sperm-oocyte adhesion is suppressed, which will cause impaired fusion between sperm and oocyte. This sperm-oocyte adhesion and subsequent fusion appears to be each independent phenomena, since the absence of β-catenin results in a reduction in the ability of sperm to adhere to an oocyte, but sperm-oocyte membrane fusion occurs normally.

Similarly, importance of interchange between stabilization and degradation of β-catenin has been described at several developmental aspects, such as mesenchymal cell proliferation[27] and primordial germ cell development[28]. Forced expression of a mutated β-catenin that is resistant to degradation causes developmental arrest at specific sites and time[27,28]. However, its deficiency has no impact on embryogenesis, probably due to compensation of other molecules that play roles similar to β-catenin[27, 28]. Probably, degradation of β-catenin that occurs at appropriate stage and place is needed for normal development of an embryo/fetus and therefore β-catenin may be an important molecule that mediates as a molecular switch in embryogenesis. Our present results showed that although the cell membrane of *β-catenin*-deficient oocytes exhibit reduced ability to adhere sperm (Fig. 3b), these oocytes could be successfully fertilized, indicating that β-catenin contributes partly to sperm-oocyte membrane adhesion, but does not play an essential role in this event. It will be claimed that ZP removal by acidic Tyrode's solution can change cell surface protein composition or carbohydrate structure, which may affect sperm-oocyte interaction to some extents. Our present data, however, clearly suggest that β-catenin degradation is associated with transition from adhesion to fusion upon interaction between sperm and oocyte.

In human trophoblastic cells, an interrelationship between cell differentiation/ fusion and reduced expression of E-cadherin has been pointed out[29]. When the isolated mononuclear cytotrophoblasts are cultured, they tend to aggregate and then fuse to form syncytia. During this process, E-cadherin is detectable at the cell-cell contact sites of an aggregate. However, the fusing cytotrophoblasts (but not non-fusing cytotrophoblasts) exhibit marked reduction in the level of E-cadherin. Notably, exposure of the non-fusing cells to 8-bromo cyclic AMP causes reduced expression of E-cadherin, and induces their cellular fusion and syncytium formation. These results suggest that down-regulation of E-cadherin gene expression coincides with cell fusion, and evoke us to suppose that remodeling of the adhesion complex on the cell surface would induce subsequent cell fusion. Beside E-cadherin, junctional proteins found in tight and adherens junctions such as integral membrane, adaptor, regulator and signaling proteins are recently thought to be important as epithelial and endothelial barriers[30]. They can reversibly increase paracellular transport and drug delivery with less toxicity, indicating that alteration in lipid composition at cell surface membrane, as exemplified by alteration of cholesterol efflux, results in modulation of cellular junctions. Based on these results, we consider that remodeling or degradation of adhesion complex may change lipid composition in a cell membrane, which will then provide microenvironments where cell fusion occurs.

When the fusion step is genetically defective, sperm never fuses with the partner oocyte, as previously shown by using *CD9*-deficient oocytes and *Izumo1*-deficient sperm[3,5,6]. Furthermore, we showed that the presence or absence of β-catenin in oocytes does not affect the expression and localization of CD9 (see Supplementary Fig. S5). In addition, we also observed that the presence or absence of CD9 does not affect the change of β-catenin localization in oocytes before and after adhesion to sperm (see Fig. 4d, e). A couple of these results suggest that β-catenin is independent from CD9 tetraspanin network. These findings evoked us to suppose that the adhesion step may be distinguishable from the fusion step in mammalian fertilization. Interestingly, Jégou *et al.* (2011) recently demonstrated that CD9 is indeed involved in the sperm-egg binding step. This suggests a possible role of CD9 in sperm-oocyte adhesion, but does not exclude the previous finding that CD9 is involved in fusion[31]. Although further investigation on the role of CD9 molecule in sperm-oocyte adhesion and subsequent fusion is needed, it seems likely at present that CD9 may be involved in maintaining the strength of adhesion force on the oocyte cell membrane. Its absence would cause unstable adhesion force, resulting in decreased fertilizing ability of sperm.

In conclusion, we have shown that 1) β-catenin plays a role in sperm-oocyte membrane adhesion upon fertilization; and 2) β-catenin is also involved in the transition of membrane adhesion to fusion, a phenomenon essential for fertilization, and proteasome-mediated regulation of β-catenin is important in such sperm-oocyte fusion.

Methods

Antibodies. Two mAbs against mouse E-cadherin used for immunostaining and immunoblotting (No. ECCD-2; Takara-Bio) and immunoprecipitation (No. 36; BD). Two mAbs against mouse β-catenin were used for immunoprecipitation (No. C2206; Sigma) and immunostaining (No. 15B8; Sigma). A mAb against β-catenin (No. 14; BD) was used for immunoblotting. A polyclonal antibody against mouse α-catenin

(No. C2081; Sigma), Cy3-conjugated mAb against C-terminal peptide conserved in β- and γ-actin isoforms (No. AC-40; Sigma), and FITC-conjugated mAb against β-tubulin (No. TUB2.1; Sigma) were used. A mAb against N-cadherin was used for immunoblotting (No. 32; BD). ECCD-2, which recognizes an epitope in the extracellular region of E-cadherin, bind to E-cadherin on the cell membrane without permeabilization[32].

Immunostaining. Mouse oocytes were collected from oviducts of 8- to 12-week-old C57BL/6N superovulated mice (Japan SLC Inc.). The oocytes were fixed for 20 min at room temperature in a solution (termed PFA-GLA-PVP) containing 2% paraformaldehyde (PFA), 0.1% glutaraldehyde (GLA) and 0.1% polyvinylpyrolidone (PVP). After washing in phosphate-buffered saline (PBS), they were permeabilized with 1% Triton X-100 in PBS, and washed 3 times in PBS. The oocytes were then incubated with the primary antibodies (Abs) (2.5 μg/ml) in HEPES-buffered saline (HBS) containing 10 mM HEPES (pH 8.0), 0.15 M NaCl and 3% fetal bovine serum (FBS) for 2 h at 4°C. These oocytes were next treated with the secondary Abs (1.25 μg/ml), Alexa488- or Alexa546-conjugated IgG (Molecular Probes), and washed 3 times in HBS. Mouse sperm were also isolated from the cauda epididymides of 8- to 12-week-old C57BL/6N male mice by teasing them in TYH medium[33], and immunostained as described above. In addition, sperm were collected from 24-week-old KAT strain[16] males of the *Suncus murinus*, kindly provided by Dr. Senichi Oda and immunostained as described above. These immunostained sperm were then counterstained with DAPI (WAKO) at the final concentration of 10 μg/ml in HBS for 30 min at 4°C, and washed 3 times by transfer to HBS.

Sectioned fluorescent images were captured by a confocal microscope (LSM 510 model; Carl Zeiss), and transformed into three-dimensional (3D) images by LSM Image Brower Version 4.2.0.121. The fluorescence intensities of target proteins were then measured based on the 3D images (Supplementary Fig. S1d, e; Fig. 1b), and compared between latA-untreated and -treated oocytes (Fig. 1d), unpermeabilized and permeabilized sperm (Fig. 2c, d), and oocytes and sperm before and after membrane adhesion (Fig. 4a–c). All animal experiments were performed according to protocols approved by the Institutional Animal Care and Use Committee at the National Institute for Child Health and Development.

Immunoblotting and immunoprecipitation. The sperm suspension (ca. 3.0×10^6 cells) prepared from C57BL/6N males was collected by centrifugation, as described by Inoue *et al.*[3] A total of 200 oocytes were collected and then lysed in Laemmli's SDS sample buffer, boiled, resolved in SDS-PAGE on an 8% acrylamide gel, and immunoblotted as described previously[34]. Mouse embryonic carcinoma P19 cells[35] were were used as a positive control. For immunoprecipitation, Sakakibara *et al.*[34] describe this procedure in more detail citing references[36]. Proteins from sperm (ca. 3.0×10^6 cells) (Fig. 2b) or 905 oocytes (Fig. 1c) were immunoprecipitated with Abs (2.5 μg/ml) for 6 h at 4°C. The presence of β-tubulin was detected and used as an internal loading control.

Actin disassembly induced by latA treatment. Mouse oocytes collected from oviducts of superovulated mice were incubated in TYH medium containing 10 μM latA (Molecular Probes) for 1 h at 37°C, and fixed in PFA-GLA-PVP solution. After permeabilization with 1% Triton X-100, oocytes were doubly immunostained by mAbs against actin and β-catenin as mentioned in the 'Immunostaining' section. The fluorescence intensities at the equator, as indicated by dotted lines, were then analyzed as described in the 'Immunostaining' section.

Generation of mice with gene-ablated oocytes. To produce oocytes with a single gene deleted, floxed mutant mice for *E-cadherin*[17], *β-catenin*[18] or *α-catenin* gene[19] were cross-mated with transgenic (Tg) mice expressing *cre-recombinase* in an oocyte-specific manner under the control of oocyte-specific ZP protein 3 (ZP3) promoter ($Tg^{ZP3\text{-}cre/+}$), kindly provided by Dr. Barbara B. Knowles[37]. The F1 offspring, so-called $E\text{-}cadherin^{floxed/floxed}Tg^{ZP3\text{-}cre/+}$, $\beta\text{-}catenin^{floxed/floxed}Tg^{ZP3\text{-}cre/+}$ and $\alpha\text{-}catenin^{floxed/floxed}Tg^{ZP3\text{-}cre/+}$, were propagated through brother-sister mating. The presence of the *cre-recombinase* gene in these offspring was detected by PCR analysis using the following set of primers: Cre-S (5'-TGATGAGGTTCGCAAGAACC-3'; nucleotide no. 170 to 189 (GenBank Accession no. AB449974.1)) and Cre-A (5'-CCATGAGTGAACGAACCTGG-3'; nucleotide no. 539 to 558 (GenBank Accession no. AB449974.1)); this primer set yielded a band of 389 bp.

Determination of litter size and *in vitro* fertilization (IVF). To determine the litter size, the number of pups delivered from an 8- to 12-week-old female (offspring of $\beta\text{-}catenin^{floxed/floxed}Tg^{ZP3\text{-}cre/+}$ mice) was recorded after mating for two months by placing an 8- to 12-week-old C57BL/6N male in the cage.

For IVF, oocytes were collected from the oviductal ampulla region of superovulated $\beta\text{-}catenin^{floxed/floxed}Tg^{ZP3\text{-}cre/+}$ females (8 to 12 weeks old) 14 to 16 h after hCG injection, and placed in a 30-μl drop of TYH medium covered with paraffin oil (Nacalai) equilibrated with 5% CO_2 in air at 37°C. Sperm collected from the epididymides of 8- to 12-week-old C57BL/6N males were induced to capacitate by incubating in TYH medium for 90 min in an atmosphere of 5% CO_2 in air at 37°C before insemination. The final concentration of sperm added to the oocytes was 1.5×10^5 sperm/ml. The oocytes collected from *floxed/floxed* mice were also inseminated with C57BL/6N sperm as a control.

To count the number of sperm fused to an oocyte, cumulus cells were dispersed from oocytes by incubating them for 10 min at 37°C in TYH medium containing hyaluronidase (300 μg/ml; Merk4Biosciences), and then the oocytes were denuded of the ZP by brief incubation in acid Tyrode's solution (Sigma). The 'zona-free' oocytes were preincubated with DAPI at the final concentration of 10 μg/ml in TYH medium for 20 min at 37°C, and washed 3 times by being transferred to separate drops of TYH medium. DAPI is a fluorescent dye that can slowly permeate the living cell membrane (semi-permeable) and hardly leaks out of cells after washing, relative to Hoechst33342 (permeable), as shown in Invitrogen's instructions. This preincubation procedure with DAPI enables the staining of only fused sperm nuclei, probably through a mechanism in which the dye present within an oocyte is transferred to fused sperm upon membranous fusion. C57BL/6N sperm (ca. 1.5×10^5 sperm/ml) were added to a 30-μl drop of TYH medium containing 30 DAPI-treated 'zona-free' oocytes and then the dish was incubated for 1 h at 37°C. After incubation, the oocytes were fixed with PFA-GLA-PVP solution for 20 min at room temperature. The rate of oocytes fused with sperm was determined by counting DAPI-transferred sperm on an oocyte under a fluorescence microscope. In this case, oocytes fused with sperm were defined as those with at least one DAPI-positive sperm. Moreover, in a separate group in which 'zona-intact' oocytes were incubated with sperm for 24 h at 37°C and then stained by DAPI, the rate of those oocytes to develop to the two-cell stage was determined under a stereoscopic microscope without fixation.

To count the number of sperm adhered to an oocyte, cumulus cells were dispersed from oocytes in TYH medium containing hyaluronidase (Merk4Biosciences), and the oocytes were denuded of the ZP by incubation in acid Tyrode's solution (Sigma). The C57BL/6N sperm (ca. 1.5×10^5 sperm/ml) were added to a 30-μl drop of TYH medium containing 30 'zona-free' oocytes and then the dish was incubated for 1 h at 37°C. After incubation, the oocytes were fixed with a PFA-GLA-PVP solution and stained with DAPI. The number of sperm adhered to an oocyte was determined by counting DAPI-positive sperm on an oocyte.

Membrane localization of β-catenin before and after membrane adhesion. To observe the localization of β-catenin before and after membrane adhesion, oocytes were collected as mentioned in the 'Determination of litter size and IVF' section. After ZP removal, 'zona-free' oocytes were incubated with C57BL/6N epididymal sperm (ca. 1.5×10^5 sperm/ml) in a 30-μl drop of TYH medium for 30 min at 37°C. The oocytes adhered to sperm, oocytes before sperm adhesion, and epididymal sperm were fixed by placing them in PFA-GLA-PVP solution, washed, and immunostained with a mAb against β-catenin and DAPI, as described in the 'Immunostaining' section.

IVF of oocytes treated with UBE1-41. To study the effect of UBE1-41 on sperm-oocyte fusion, oocytes were collected as mentioned in the 'Determination of litter size and IVF' section, incubated in a 30-μl drop of TYH medium containing UBE1-41 (Biogenova) and DAPI for 1 h at 37°C, and washed with TYH medium. After ZP removal, 'zona-free' oocytes (30 oocytes) were incubated with C57BL/6N epididymal sperm (ca. 1.5×10^5 sperm/ml) in a 30-μl drop of TYH medium for 30 min at 37°C. These oocytes were then fixed by placing them in PFA-GLA-PVP solution, washed, and immunostained with a mAb against β-catenin, as described in the 'Immunostaining' section. The 'zona-free' oocytes were similarly treated in a medium without UBE1-41 and used as the control. The relative rate of oocytes fused with sperm was compared between UBE1-41-treated and untreated oocytes.

1. Ikawa, M., Inoue, N., Benham, A. M., and Okabe, M. Fertilization: a sperm's journey to and interaction with the oocyte. *J Clin Invest* **120**, 984–994 (2010).
2. Mitamura, T. *et al.* The 27-kD diphtheria toxin receptor-associated protein (DRAP27) from vero cells is the monkey homologue of human CD9 antigen: expression of DRAP27 elevates the number of diphtheria toxin receptors on toxin-sensitive cells. *J Cell Biol* **118**, 1389–1399 (1992).
3. Inoue, N., Ikawa, M., Isotani, A., and Okabe, M. The immunoglobulin superfamily protein Izumo is required for sperm to fuse with eggs. *Nature* **434**, 234–238 (2005).
4. Miyado, K. *et al.* Requirement of CD9 on the egg plasma membrane for fertilization. *Science* **287**, 321–324 (2000).
5. Le Naour, F. *et al.*, Severely reduced female fertility in CD9-deficient mice. *Science* **287**, 319–321 (2000).
6. Miyado, K. *et al.* The fusing ability of sperm is bestowed by CD9-containing vesicles released from eggs in mice. *Proc Natl Acad Sci USA* **105**, 12921–12926 (2008).
7. Barraud-Lange, V. *et al.* Transfer of oocyte membrane fragments to fertilizing spermatozoa. *FASEB J* **21**, 3446–3449 (2007).
8. Runge, K. E. *et al.* Oocyte CD9 is enriched on the microvillar membrane and required for normal microvillar shape and distribution. *Dev Biol* **304**, 317–325 (2007).
9. Yamada, S. *et al.* Deconstructing the cadherin-catenin-actin complex. *Cell* **123**, 889–901 (2005).
10. De Vries, W. N. *et al.* Maternal beta-catenin and E-cadherin in mouse development. *Development* **131**, 4435–4445 (2004).
11. Nagafuchi, A., Ishihara, S., and Tsukita, S. The roles of catenins in the cadherin-mediated cell adhesion: functional analysis of E-cadherin-alpha catenin fusion molecules. *J Cell Biol* **127**, 235–245 (1994).
12. Behrens, J. *et al.* Functional interaction of beta-catenin with the transcription factor LEF-1. *Nature* **382**, 638–642 (1996).
13. Fulka, J., Jr., Flechon, B., and Flechon, J. E. Fusion of mammalian oocytes: SEM observations of surface changes. *Reprod Nutr Dev* **29**, 551–557 (1989).